

# IFN $\gamma$ binding to extracellular matrix prevents fatal systemic toxicity

Received: 21 June 2022

Accepted: 28 December 2022

Published online: 2 February 2023

Check for updates

Josephine Kemna<sup>1</sup>, Evelyne Gout<sup>2</sup>, Leon Daniau<sup>3,4</sup>, Jessica Lao<sup>3,4</sup>,  
Kristoffer Weißert<sup>3,4,5</sup>, Sandra Ammann<sup>3,5</sup>, Ralf Kühn<sup>6</sup>,  
Matthias Richter<sup>7</sup>, Christine Molenda<sup>7</sup>, Anje Sporberr<sup>7</sup>, Dario Zocholl<sup>8</sup>,  
Robert Klopffleisch<sup>9</sup>, Anja Schütz<sup>10</sup>, Hugues Lortat-Jacob<sup>2</sup>, Peter Aichele<sup>3,5</sup>,  
Thomas Kammertoens<sup>1,11,12</sup> & Thomas Blankenstein<sup>1,12</sup>

Interferon- $\gamma$  (IFN $\gamma$ ) is an important mediator of cellular immune responses, but high systemic levels of this cytokine are associated with immunopathology. IFN $\gamma$  binds to its receptor (IFN $\gamma$ R) and to extracellular matrix (ECM) via four positively charged C-terminal amino acids (KRKR), the ECM-binding domain (EBD). Across evolution, IFN $\gamma$  is not well conserved, but the EBD is highly conserved, suggesting a critical function. Here, we show that IFN $\gamma$  lacking the EBD (IFN $\gamma^{\Delta KRKR}$ ) does not bind to ECM but still binds to the IFN $\gamma$ R and retains bioactivity. Overexpression of IFN $\gamma^{\Delta KRKR}$  in tumors reduced local ECM binding, increased systemic levels and induced sickness behavior, weight loss and toxicity. To analyze the function of the EBD during infection, we generated IFN $\gamma^{\Delta KRKR}$  mice lacking the EBD by using CRISPR–Cas9. Infection with lymphocytic choriomeningitis virus resulted in higher systemic IFN $\gamma^{\Delta KRKR}$  levels, enhanced sickness behavior, weight loss and fatal toxicity. We conclude that local retention of IFN $\gamma$  is a pivotal mechanism to protect the organism from systemic toxicity during prolonged immune stimulation.

Throughout evolution, the immune system has evolved increasingly powerful weapons against pathogens. The price of the arms race between the immune system and pathogens is the risk of overshooting immune responses and subsequent immunopathology<sup>1</sup>. Therefore, counteracting mechanisms, such as regulatory T cells or immune checkpoints that restrict effector T cells, have evolved, which diminish effector function<sup>2–4</sup>. Arguably, cytokines, such as interferon- $\gamma$  (IFN $\gamma$ ), are the most toxic components of the immune response if they are

released systemically in large amounts and for extended periods of time<sup>5,6</sup>. Infections usually occur locally, and IFN $\gamma$  is secreted locally by T cells after recognition of antigen-presenting target cells and can spread around 800  $\mu$ m, the equivalent of 30–40 cell layers<sup>7,8</sup>.

In addition to binding to the ubiquitously expressed IFN $\gamma$  receptor (IFN $\gamma$ R) with an affinity ( $K_d$ ) of 0.5 nM, IFN $\gamma$  also binds to the heparan sulfate (HS) moiety of the extracellular matrix (ECM) with an affinity of 1.5 nM (Fig. 1a)<sup>9</sup>. Binding to the ECM is mediated by four positively

<sup>1</sup>Max-Delbrück Center for Molecular Medicine in the Helmholtz Association, Molecular Immunology and Gene Therapy, Berlin, Germany. <sup>2</sup>Institut de Biologie Structurale, UMR 5075, University Grenoble Alpes, Centre National de la Recherche Scientifique, Commissariat à l'Énergie Atomique et aux Énergies Alternatives, Grenoble, France. <sup>3</sup>Institute for Immunodeficiency, Medical Center—University of Freiburg, Faculty of Medicine, University of Freiburg, Freiburg, Germany. <sup>4</sup>Faculty of Biology, Albert-Ludwigs-University of Freiburg, Freiburg, Germany. <sup>5</sup>Center for Chronic Immunodeficiency (CCI), Medical Center—University of Freiburg, Faculty of Medicine, University of Freiburg, Freiburg, Germany. <sup>6</sup>Transgenic Core Facility, Max-Delbrück Center for Molecular Medicine in the Helmholtz Association, Berlin, Germany. <sup>7</sup>Advanced Light Microscopy Core Facility, Max-Delbrück Center for Molecular Medicine in the Helmholtz Association, Berlin, Germany. <sup>8</sup>Charité—Universitätsmedizin Berlin, Corporate Member of Freie Universität Berlin and Humboldt-Universität zu Berlin, Institute of Biometry and Clinical Epidemiology, Berlin, Germany. <sup>9</sup>Department of Veterinary Medicine, Institute of Veterinary Pathology, Freie Universität Berlin, Berlin, Germany. <sup>10</sup>Protein Production & Characterization Core Facility, Max-Delbrück Center for Molecular Medicine in the Helmholtz Association, Berlin, Germany. <sup>11</sup>Institute of Immunology, Charité Universitätsmedizin, Campus Buch, Berlin, Germany.

<sup>12</sup>These authors jointly supervised this work: Thomas Kammertoens, Thomas Blankenstein. e-mail: [tblank@mdc-berlin.de](mailto:tblank@mdc-berlin.de)

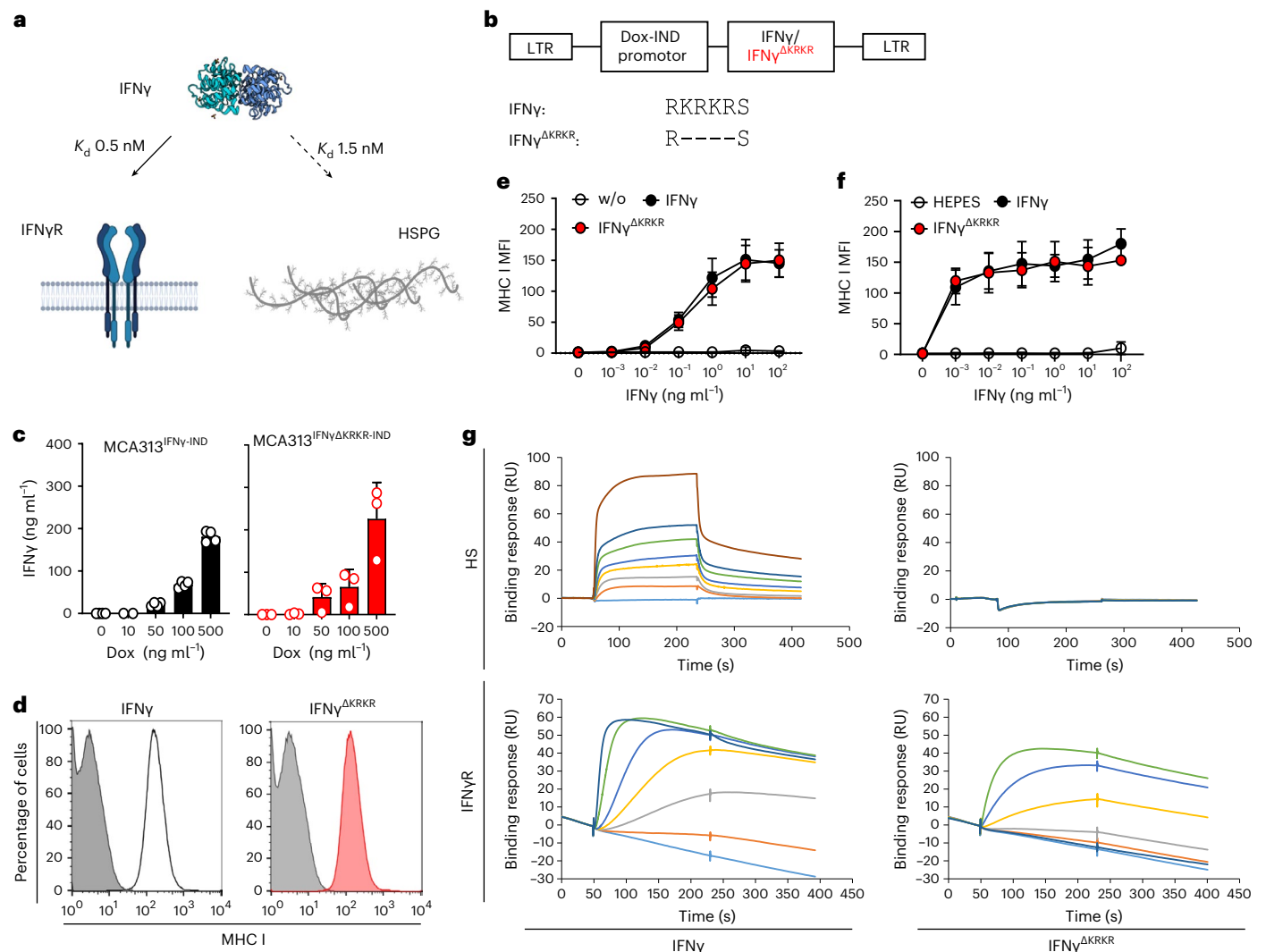


**Fig. 1 | The evolutionarily conserved KRKR motif of IFN $\gamma$  is necessary for binding to HS. a**, IFN $\gamma$  binds to the IFN $\gamma$ R and HSPG. **b**, Construct flanked by long terminal repeats (LTR) for generation of MCA313 cancer cells with Dox-inducible (Dox-IND) expression of different IFN $\gamma$  variants (MCA313<sup>IFN $\gamma$ -IND</sup> and MCA313<sup>IFN $\gamma^{\Delta KRKR}$ -IND</sup>). **c**, Dox-dependent expression of IFN $\gamma$  variants in MCA313 cells in vitro. The data show the means + s.d. of  $n = 4$  (MCA313<sup>IFN $\gamma$ -IND</sup>) and  $n = 3$  (MCA313<sup>IFN $\gamma^{\Delta KRKR}$ -IND</sup>) experiments. **d**, Upregulation of MHC class I (H-2K<sup>b</sup>/H-2D<sup>b</sup>) molecules on B16-F10 cells after treatment with 1 ng ml<sup>-1</sup> IFN $\gamma$  (left) or IFN $\gamma^{\Delta KRKR}$  (right). B16-F10 cells were cultured for 48 h with supernatants from MCA313 (gray), MCA313<sup>IFN $\gamma$ -IND</sup> (black line) or MCA313<sup>IFN $\gamma^{\Delta KRKR}$ -IND</sup> (red histogram) cells, respectively, and analyzed by flow cytometry. Shown is one representative

experiment out of four. **e**, IFN $\gamma$  or IFN $\gamma^{\Delta KRKR}$  dose-dependent upregulation of MHC class I on B16-F10 cells. Shown are means  $\pm$  s.d. of four experiments; MFI, mean fluorescence intensity. **f**, Biological activity of recombinant (*E. coli*-produced) IFN $\gamma$  and IFN $\gamma^{\Delta KRKR}$  variants as indicated and analyzed in **e**. Shown are means  $\pm$  s.d. of two individual biological experiments. **g**, IFN $\gamma$  (left) or IFN $\gamma^{\Delta KRKR}$  (right) was injected over an HS-activated surface (top) or an IFN $\gamma$ R1-activated surface (bottom) over 180 s, and the binding response in resonance units (RU) was recorded as a function of time. Each set of sensorgrams was obtained with IFN $\gamma$  at (from bottom to top) 0, 25, 50, 75, 100, 150, 200 and 500 nM for the HS surface and at 0, 1, 2.5, 5, 10, 25 and 50 nM for the IFN $\gamma$ R1 surface.

charged amino acids (KRKR) at the C terminus of IFN $\gamma$ . The biological role of IFN $\gamma$  binding to the ECM is unknown. On the basis of cell culture experiments, different hypotheses were developed. One hypothesis is that the C-terminal part of IFN $\gamma$  (amino acids 95–133 containing the KRKR motif) is essential for biological activity<sup>10</sup>. It was also suggested that the KRKR motif acts as a nuclear localization signal<sup>11</sup> or facilitates binding to the IFN $\gamma$ R<sup>12</sup>. Because of the strong evolutionary conservation of the KRKR motif in the IFN $\gamma$  protein, we investigated its relevance in in vivo models.

## Results

### The KRKR motif of IFN $\gamma$ is conserved

Comparing the IFN $\gamma$  protein sequences between 50 vertebrate species covering 450 million years of evolution showed little conservation and overall low homology (Table 1 and Extended Data Table 1), an observation that is in line with reports showing high species specificity of IFN $\gamma$

and no conserved ligand–IFN $\gamma$ R interaction motifs<sup>13</sup>. Mouse and human IFN $\gamma$ , for example, are 41% homologous at the amino acid level and do not cross-react<sup>14</sup>. By contrast, the C-terminal KRKR motif is highly conserved throughout evolution, suggesting an essential biological function (Table 1 and Extended Data Table 1). In several species distantly related to mammals (for example, elephant shark, zebra fish, American bullfrog or alligator), deviations from the KRKR motif were detected. In these cases, amino acids of the KRKR motif were substituted without exception by positively charged amino acids, further suggesting an important evolutionary role of this motif.

### IFN $\gamma^{\Delta KRKR}$ loses ECM binding but not IFN $\gamma$ R binding

We were concerned that deletion of the KRKR motif would abolish not only ECM binding but also the biological activity of IFN $\gamma$ . To test if IFN $\gamma^{\Delta KRKR}$  (lacking the KRKR motif) retained biological activity, we

**Table 1 | IFN $\gamma$  sequences across five different taxa**

Organism	Motif sequence	Identity to mouse IFN $\gamma$ (%)	Common name	Taxon
<i>Mus musculus</i>	<b>RKRKRS</b>	100	Mouse	Mammalia
<i>Rattus norvegicus</i>	<b>RKRKRS</b>	83	Rat	
<i>Homo sapiens</i>	<b>GKRKRS</b>	41	Human	
<i>Ornithorhynchus anatinus</i>	<b>RKKRRS</b>	29	Platypus	
<i>Taeniopygia guttata</i>	<b>YKRKRS</b>	33	Zebra finch	Aves
<i>Anas platyrhynchos</i>	<b>SKRKRS</b>	29	Mallard	
<i>Pelodiscus sinensis</i>	<b>NKRKRS</b>	30	Chinese soft-shelled turtle	Reptilia
<i>Xenopus tropicalis</i>	<b>VKKRKL</b>	25	Tropical clawed frog	Amphibia
<i>Lithobates catesbeiana</i>	<b>VRRKRG</b>	22	American bullfrog	
<i>Oncorhynchus mykiss</i>	<b>NRRKRR</b>	27	Rainbow trout	Bony fish
<i>Danio rerio</i>	<b>ERKRRQ</b>	22	Zebra fish	
<i>Callorhynchus milii</i>	<b>GRRRRR</b>	23	Elephant shark	Cartilaginous fish

IFN $\gamma$  sequences across five different taxa and 450 million years of evolution showing a low degree of homology but high conservation of the KRKR motif at the C terminus. Deviations from the mouse KRKR motif are marked by underlining. The common amino acid single-letter code is shown. All 50 species are shown in Extended Data Table 1.

transduced MCA313 fibrosarcoma cells<sup>15</sup> with retroviruses that allowed for doxycycline (Dox)-induced expression of either IFN $\gamma$  or IFN $\gamma^{\Delta\text{KRKR}}$  (Fig. 1b). Both cytokines were inducibly expressed in similar amounts (Fig. 1c). Additionally, IFN $\gamma$  and IFN $\gamma^{\Delta\text{KRKR}}$  induced upregulation of H-2K<sup>b</sup>/H-2D<sup>b</sup> molecules on B16-F10 melanoma cells in a similar and concentration-dependent manner (Fig. 1d,e).

We expressed and purified recombinant IFN $\gamma$  and IFN $\gamma^{\Delta\text{KRKR}}$  in *Escherichia coli*, and both cytokines upregulated the expression of major histocompatibility complex class I (MHC class I) on B16-F10 cells (Fig. 1f). We then analyzed the interactions of IFN $\gamma$  and IFN $\gamma^{\Delta\text{KRKR}}$  with IFN $\gamma$ R1, the ligand-binding chain of the heterodimeric IFN $\gamma$ R and HS by surface plasmon resonance (SPR). Binding of IFN $\gamma$  and IFN $\gamma^{\Delta\text{KRKR}}$  to an IFN $\gamma$ R1 surface or to an HS surface was measured at various ligand concentrations. Deletion of the ECM-binding domain (EBD; IFN $\gamma^{\Delta\text{KRKR}}$ ) decreased the on rate of the binding response to IFN $\gamma$ R1 (Fig. 1g), in agreement with previous studies demonstrating that the basic C-terminal residues of the cytokine enhance the on rate of IFN $\gamma$  binding to IFN $\gamma$ R1 (ref. 12) but do not prevent the formation of the complex nor its stability. By contrast, deletion of the EBD completely abrogated binding to HS (Fig. 1g), which was also supported by previous nuclear magnetic resonance-based studies showing that IFN $\gamma$  amino acids experiencing chemical shift variation after binding to HS are exclusively localized in the basic motif of the cytokine C terminus<sup>16</sup>. Thus, IFN $\gamma$  binds to both IFN $\gamma$ R1 and HS, whereas the IFN $\gamma^{\Delta\text{KRKR}}$  variant retains IFN $\gamma$ R binding and biological activity but loses ECM binding.

### Reduced colocalization of IFN $\gamma^{\Delta\text{KRKR}}$ -GFP and ECM

Direct evidence that the KRKR motif mediates ECM binding in vivo is lacking; thus, we analyzed whether IFN $\gamma$  and HS colocalize in vivo. For IFN $\gamma$  visualization in tissue, IFN $\gamma$ -green fluorescent protein (GFP) fusion proteins were used because detection of IFN $\gamma$  using antibodies can be misleading<sup>17</sup>, and, of note, we wished to detect extracellular, HS-bound IFN $\gamma$ . Recombinant fusion proteins IFN $\gamma$ -GFP and IFN $\gamma^{\Delta\text{KRKR}}$ -GFP were similarly bioactive in upregulating MHC class I expression on B16-F10 cells (Extended Data Fig. 1a). As measured by SPR, IFN $\gamma^{\Delta\text{KRKR}}$ -GFP had retained IFN $\gamma$ R binding but lost HS binding, while IFN $\gamma$ -GFP bound to both IFN $\gamma$ R and HS (Extended Data Fig. 1b). MCA313 cells were generated and secreted similar amounts of IFN $\gamma$ -GFP (MCA313<sup>IFN $\gamma$ -GFP-IND</sup>) or IFN $\gamma^{\Delta\text{KRKR}}$ -GFP (MCA313<sup>IFN $\gamma^{\Delta\text{KRKR}}$ -GFP-IND</sup>) in a Dox-inducible manner (Fig. 2a,b). Tumors were established in *Ifng<sup>-/-</sup>/Ifngr1<sup>-/-</sup>* mice, which prevented IFN $\gamma$ R binding and excluded competition with endogenous IFN $\gamma$  for HS binding. Expression of IFN $\gamma$ -GFP and IFN $\gamma^{\Delta\text{KRKR}}$ -GFP was induced by Dox for a minimum of 3 d when tumors reached 200–300 mm<sup>3</sup>. Then, Dox was withdrawn for 48 h to stop cytokine production, and tumor tissues were analyzed for colocalization between IFN $\gamma$ -GFP and HS. Tumor sections were stained with antibodies specific to CD146 and HS proteoglycan (HSPG) to visualize endothelial cells and HS (Extended Data Fig. 1c,d). The HSPG antibody (clone A7L6) binds to perlecan domain IV, a major HSPG constituent of the basement membrane in blood vessels<sup>18</sup>. This way, we could

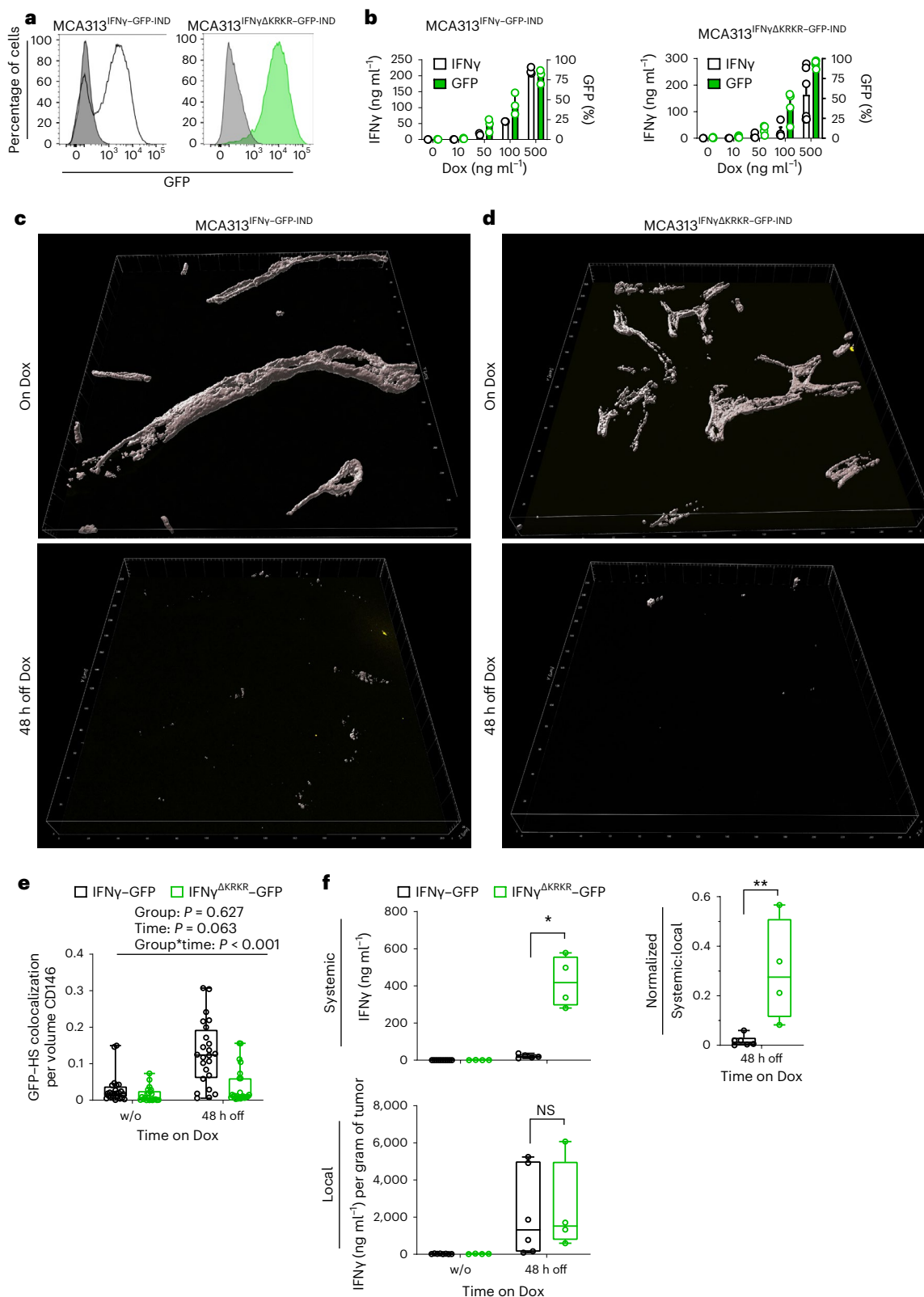
### Fig. 2 | IFN $\gamma$ colocalizes with HS in vivo and is retained locally.

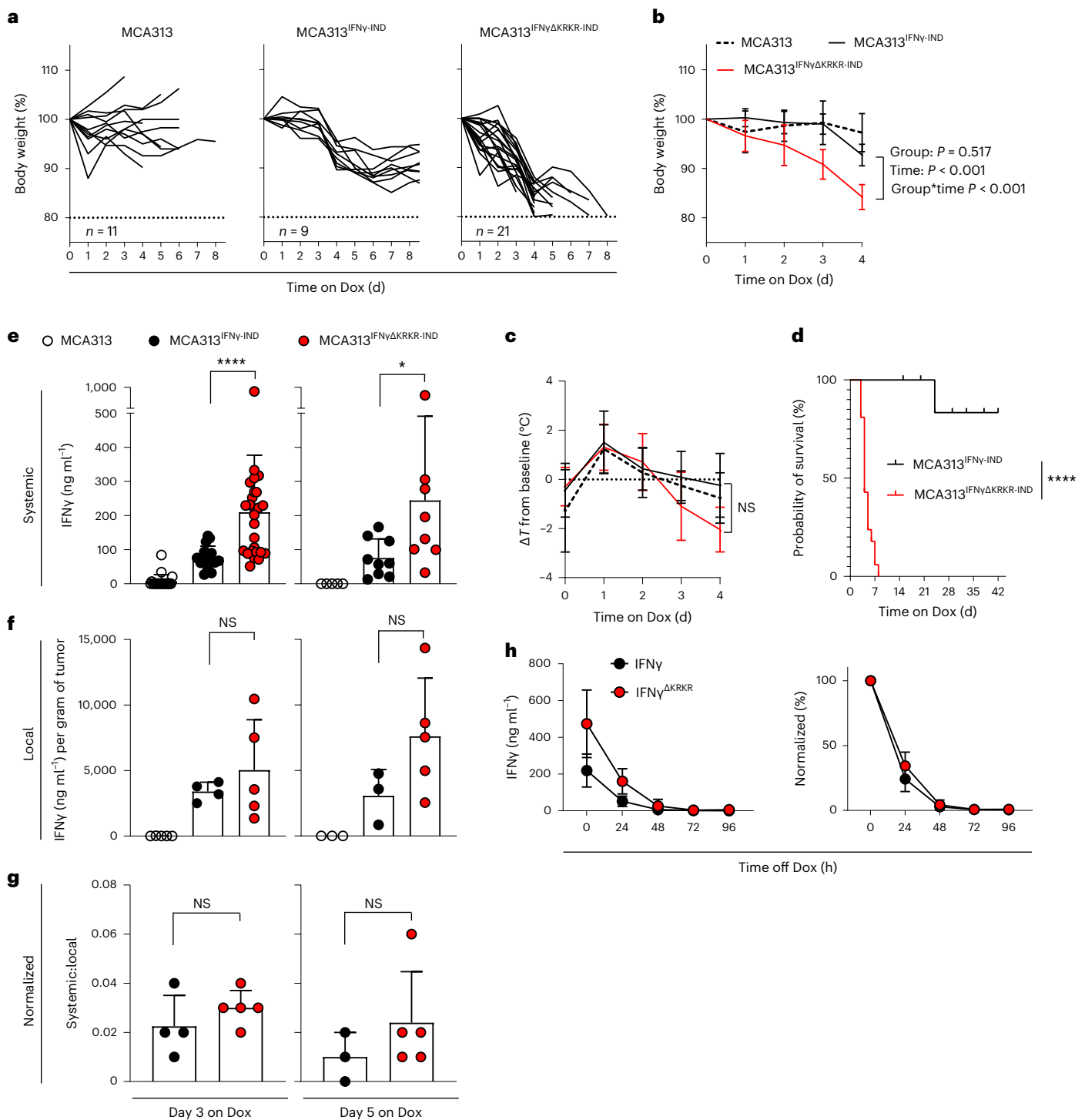
**a**, Representative examples of inducible expression of IFN $\gamma$ -GFP (left, black line) and IFN $\gamma^{\Delta\text{KRKR}}$ -GFP (right, green histogram) in MCA313 cells after stimulation with 500 ng ml<sup>-1</sup> Dox. Gray histograms show absence of expression in the absence of Dox. **b**, Dox-dependent expression of IFN $\gamma$ -GFP and IFN $\gamma^{\Delta\text{KRKR}}$ -GFP in MCA313 cells in vitro. Data are shown as mean and s.d. of  $n = 2-4$  (MCA313<sup>IFN $\gamma$ -GFP-IND</sup>) and  $n = 4-6$  (MCA313<sup>IFN $\gamma^{\Delta\text{KRKR}}$ -GFP-IND</sup>) experiments. **c,d**, *Ifng<sup>-/-</sup>/Ifngr1<sup>-/-</sup>* mice were injected with either MCA313<sup>IFN $\gamma$ -GFP-IND</sup> (c) or MCA313<sup>IFN $\gamma^{\Delta\text{KRKR}}$ -GFP-IND</sup> cells (d). Dox was administered via the drinking water (on Dox) when tumors reached 200–300 mm<sup>3</sup>. Tumors were induced for a minimum of 3 d, and Dox was withdrawn (48 h off Dox). Three-dimensional surface reconstructions of the colocalization channel of 16- $\mu$ m sections acquired by confocal microscopy from tumor tissue are shown. Using Imaris, colocalization channels were calculated from colocalizing voxels of GFP and HS within the CD146 volume. Shown are representative volumes from on Dox and 48 h after Dox withdrawal (48 h off). Representative stainings of the same specimens are depicted in Extended Data

Fig. 1c,d. Whole 3D z stacks are also in Supplementary Video 1. **e**, Colocalization as determined by normalizing the calculated colocalization volume for GFP and HS to the CD146 volume. Five to six confocal z stacks were acquired from four mice per group. Volumes were calculated using Imaris 9.7.2. **f**, Serum levels (systemic) and tumor levels (local) of IFN $\gamma$ -GFP variants in *Ifng<sup>-/-</sup>/Ifngr1<sup>-/-</sup>* mice were determined by ELISA 48 h after Dox withdrawal. Mice without Dox served as controls (w/o). The fraction of the respective IFN $\gamma$ -GFP variant systemically available was determined by normalizing systemic levels to local levels. Data from  $n = 4-10$  mice per group from two independent experiments are shown, and data from individual mice are plotted. Median values are shown as the center lines, minima are the lower limits, maxima are the upper limits, and quartiles are the bounds of boxes. Statistical analyses were performed using the Mann-Whitney test (two sided) or a linear mixed model with random intercept for each individual and an interaction effect between time and group (e); NS, not significant; \* $P = 0.0159$  and \*\* $P = 0.0095$ .

exclude residual GFP signal from the cancer cells. Immunohistochemical analysis of tumor tissue revealed tenfold more colocalization of IFN $\gamma$ -GFP voxels with HS voxels than colocalization of IFN $\gamma^{\Delta KRKR}$ -GFP voxels with HS voxels within the CD146 volume (Fig. 2c–e and Supplementary Video 1). Serum IFN $\gamma^{\Delta KRKR}$ -GFP levels were significantly higher than serum IFN $\gamma$ -GFP levels 48 h after Dox withdrawal (Fig. 2f). Local concentrations were not different between IFN $\gamma$ -GFP and

IFN $\gamma^{\Delta KRKR}$ -GFP; however, we surmise that the ECM-bound IFN $\gamma$ -GFP is less quantitatively extracted from the tumor tissue than IFN $\gamma^{\Delta KRKR}$ -GFP. The normalized systemic IFN $\gamma$ :local IFN $\gamma$  values from the same animals were significantly higher for IFN $\gamma^{\Delta KRKR}$ -GFP than for IFN $\gamma$ -GFP (Fig. 2f). We conclude that the KRKR motif mediates binding to HS in vivo and acts like a sponge to retain IFN $\gamma$  locally, thereby reducing its systemic availability.





**Fig. 3 | Locally produced IFN $\gamma$ <sup>AKRRR</sup> induces wasting disease and increases serum levels in tumor-bearing mice. **a**, Mice bearing MCA313, MCA313<sup>IFN $\gamma$</sup> -IND or MCA313<sup>IFN $\gamma$ AKRRR</sup>-IND tumors received Dox in the drinking water starting at a tumor volume of  $487 \pm 110 \text{ mm}^3$ ,  $487 \pm 95 \text{ mm}^3$  and  $516 \pm 119 \text{ mm}^3$ , respectively, and weight loss was analyzed over time. Cumulative data from four experiments are shown. **b**, Mean ( $\pm$ s.d.) weight loss in mice from **a**. **c**, Body temperature (shown as mean  $\pm$ s.d.) of four mice per group from **a** was monitored. **d**, Survival of mice in **a**. Mice reaching maximal tumor volume or end of experiment are censored. **e**, IFN $\gamma$  in the sera of mice on day 3 (left, MCA313<sup>IFN $\gamma$</sup> -IND  $n = 16$  and MCA313<sup>IFN $\gamma$ AKRRR</sup>-IND  $n = 26$ ) and day 5 (right, MCA313<sup>IFN $\gamma$</sup> -IND  $n = 9$  and MCA313<sup>IFN $\gamma$ AKRRR</sup>-IND  $n = 8$ ) for the mice depicted in **a**. **f**, Local concentrations of IFN $\gamma$  on day 3 at the tumor site were determined for MCA313<sup>IFN $\gamma$</sup> -IND ( $n = 4$ ) and MCA313<sup>IFN $\gamma$ AKRRR</sup>-IND tumor-bearing mice ( $n = 5$ ). On day 5, local IFN $\gamma$  concentrations were determined for MCA313<sup>IFN $\gamma$</sup> -IND tumor-bearing mice ( $n = 3$ ) and for MCA313<sup>IFN $\gamma$ AKRRR</sup>-IND tumor-bearing mice ( $n = 5$ ).**

**g**, Ratios of systemic to local IFN $\gamma$  levels were calculated for mice with both values available. On day 3, the systemic:local ratio in MCA313<sup>IFN $\gamma$</sup> -IND tumor-bearing mice ( $n = 4$ ) was  $0.023 \pm 0.013$  and was  $0.030 \pm 0.007$  in MCA313<sup>IFN $\gamma$ AKRRR</sup>-IND tumor-bearing mice ( $n = 5$ ). On day 5, the ratio was calculated to be  $0.010 \pm 0.010$  for MCA313<sup>IFN $\gamma$</sup> -IND tumor-bearing mice ( $n = 3$ ) and  $0.024 \pm 0.021$  for MCA313<sup>IFN $\gamma$ AKRRR</sup>-IND tumor-bearing mice ( $n = 5$ ). All values given are mean  $\pm$ s.d. **h**, Serum kinetics of different IFN $\gamma$  variants in *Ifng*<sup>-/-</sup>*Ifngr1*<sup>-/-</sup> mice bearing the respective MCA313 tumors. Mice received Dox for 3 d when tumors reached 200–400 mm<sup>3</sup> (MCA313<sup>IFN $\gamma$</sup> -IND  $n = 6$ , MCA313<sup>IFN $\gamma$ AKRRR</sup>-IND  $n = 6$ ), Dox was withdrawn, and IFN $\gamma$  serum levels were analyzed over time. Data from mice from two independent experiments are shown as mean  $\pm$ s.d. Significance was calculated using the Mantel–Cox test for survival, a Mann–Whitney test (two sided) was used for **e–g**, and a linear mixed model with random intercept for each individual and an interaction effect between time and group was used for **b** and **c**; \* $P = 0.036$  and \*\*\*\* $P \leq 0.0001$ .

### Local IFN $\gamma^{\Delta\text{KRKR}}$ expression causes severe systemic toxicity

We investigated how deletion of the EBD affects biological functions and health status in IFN $\gamma$ -competent C57BL/6N mice by local IFN $\gamma$  or IFN $\gamma^{\Delta\text{KRKR}}$  release from solid tumors. In mice with established MCA313, MCA313<sup>IFN $\gamma$ -IND</sup> or MCA313<sup>IFN $\gamma^{\Delta\text{KRKR}}$ -IND</sup> tumors, the IFN $\gamma$  variants were induced by Dox administration via the drinking water. The growth of MCA313<sup>IFN $\gamma$ -IND</sup> and MCA313<sup>IFN $\gamma^{\Delta\text{KRKR}}$ -IND</sup> tumors slowed, while MCA313 tumors progressively grew (Extended Data Fig. 2a). Within a few days, the release of IFN $\gamma^{\Delta\text{KRKR}}$  induced sickness-related behavior, as observed by reduced movement and curled body posture. IFN $\gamma^{\Delta\text{KRKR}}$  induced severe weight loss (around 20%; Fig. 3a,b) and reduced the body temperature ( $-2^\circ\text{C}$   $\Delta T$ ) within 4 d (Fig. 3c), and the mice had to be killed due to a predefined humane endpoint (Fig. 3d). By contrast, induction of IFN $\gamma$  induced mild weight loss and little change in body temperature, and mice recovered after several days (Fig. 3a–d). While differences in weight loss between both groups were statistically significant, sickness was accompanied by a wider range of temperatures (that is, higher standard deviation) so that the differences of the latter did not reach statistical significance. Severe systemic toxicity induced by IFN $\gamma^{\Delta\text{KRKR}}$  correlated with increased serum levels of the proinflammatory cytokines interleukin-1 $\beta$  (IL-1 $\beta$ ) and IL-6 (Extended Data Fig. 2b,c), which, however, again did not reach statistical significance. Local IFN $\gamma$  and IFN $\gamma^{\Delta\text{KRKR}}$  concentrations in the tumor were not different. We believe that the ECM-bound IFN $\gamma$  could not be extracted from the tumor tissue as efficiently as free IFN $\gamma$  (Fig. 3f). Serum levels of IFN $\gamma$  after Dox induction were increased about threefold on days 3 and 5 in mice harboring MCA313<sup>IFN $\gamma^{\Delta\text{KRKR}}$ -IND</sup> tumors compared to mice harboring MCA313<sup>IFN $\gamma$ -IND</sup> tumors (Fig. 3e); however, the normalized ratio of systemic to local IFN $\gamma^{\Delta\text{KRKR}}$  was increased compared to IFN $\gamma$  (Fig. 3g). To exclude the possibility that the increased systemic levels of IFN $\gamma^{\Delta\text{KRKR}}$  compared to IFN $\gamma$  were due to altered serum half-life of IFN $\gamma^{\Delta\text{KRKR}}$ , both cytokines were induced in *Ifng<sup>-/-</sup>/Ifngr1<sup>-/-</sup>* mice bearing MCA313<sup>IFN $\gamma$ -IND</sup> or MCA313<sup>IFN $\gamma^{\Delta\text{KRKR}}$ -IND</sup> tumors. After Dox withdrawal, serum levels of IFN $\gamma$  and IFN $\gamma^{\Delta\text{KRKR}}$  were analyzed over time. There was no difference in the serum half-life of both proteins (Fig. 3h). Importantly, severe systemic toxicity was also observed when IFN $\gamma^{\Delta\text{KRKR}}$ , but not IFN $\gamma$ , was induced in tumors in T cell- and B cell-deficient *Rag2<sup>-/-</sup>* mice (Extended Data Fig. 2d,e), suggesting that toxicity was not mediated by T cells. In summary, the deletion of the EBD of IFN $\gamma$  leads to fatal immunopathology caused by local expression in the tumor tissue.

### Fatal toxicity in lymphocytic choriomeningitis virus (LCMV)-infected IFN $\gamma^{\Delta\text{KRKR}}$ mice

To analyze the role of the IFN $\gamma$  KRKR motif in a virus infection model, we generated a mouse line with the KRKR motif deleted in the endogenous *Ifng* gene by using CRISPR–Cas9 technology. Two guide RNAs (gRNAs), a template lacking the KRKR sequence and CRISPR–Cas9 protein were electroporated into C57BL/6N zygotes to introduce double-strand breaks and homology-directed repair, followed by transfer into pseudopregnant mice (Fig. 4a). After sequence analysis, 8 of 31 pups born were identified to have a precise deletion of the KRKR coding sequence on both alleles, shown for three founders (Extended Data Fig. 3a). Additionally, the deletion of an *Acil* restriction site in the KRKR coding sequence was used to assess zygosity of the eight founder mice (Extended Data Fig. 3b). IFN $\gamma^{\Delta\text{KRKR}}$  mice showed no gross abnormalities and developed and bred normally. Histopathology did not identify pathologic changes or signs of neoplasia, degeneration or inflammation in IFN $\gamma^{\Delta\text{KRKR}}$  mice compared to wild-type control littermates (IFN $\gamma^{\text{wt}}$ ). Spleen tissue and blood were analyzed to assess the distribution of immune cell populations. No differences in total splenocytes between IFN $\gamma^{\Delta\text{KRKR}}$  and IFN $\gamma^{\text{wt}}$  mice were detected (Extended Data Fig. 4a). Populations of T cells, B cells, monocytes, dendritic cells and natural killer cells were detected with similar frequencies in IFN $\gamma^{\Delta\text{KRKR}}$  and IFN $\gamma^{\text{wt}}$  mice (Extended Data Fig. 4b). IFN $\gamma$  production after in vitro stimulation of peripheral blood lymphocytes or splenocytes with antibodies to CD3/CD28 was also similar (Extended Data Fig. 4c).

We tested IFN $\gamma^{\Delta\text{KRKR}}$  mice with three types of experimental stimulation known to result in a rapid increase in IFN $\gamma$  followed by a similarly rapid decrease to baseline: (1) injection of anti-CD3 (ref. 19), (2) injection of lipopolysaccharide (LPS)<sup>20</sup> or (3) rejection of solid tumors<sup>15</sup>. In both IFN $\gamma^{\Delta\text{KRKR}}$  and IFN $\gamma^{\text{wt}}$  mice, treatment with anti-CD3 and LPS induced similar rapid increases in IFN $\gamma$  serum levels and transient weight loss, followed by decreases to baseline levels within 24 h (Extended Data Fig. 4d,e). *Rag1<sup>-/-</sup>* mice bearing large established SV40 large T antigen-expressing tumors<sup>21</sup> were then treated with CD8<sup>+</sup> T cells transgenic for a T cell antigen receptor (TCR) specific for peptide I of the large T antigen (TCR-I) expressing either IFN $\gamma^{\Delta\text{KRKR}}$  or IFN $\gamma^{\text{wt}}$  (Extended Data Fig. 4f). In this model, successful T cell therapy requires IFN $\gamma$  as an effector molecule<sup>21</sup>. IFN $\gamma^{\Delta\text{KRKR}}$  and IFN $\gamma^{\text{wt}}$  TCR-I T cells similarly expanded after transfer and eradicated the tumor with similar rejection kinetics (maximal predicted probability of 63% for a group difference at any time; Extended Data Fig. 4g,h). In mice treated with IFN $\gamma^{\Delta\text{KRKR}}$  or IFN $\gamma^{\text{wt}}$  TCR-I T cells, IFN $\gamma$  serum levels with similar kinetics peaked on day 4 and dropped to baseline on day 6 (Extended Data Fig. 4i). The data confirm that IFN $\gamma^{\Delta\text{KRKR}}$  has retained biological activity and that ECM binding of IFN $\gamma$  is not necessary for tumor rejection in vivo. Furthermore, in models of transient IFN $\gamma$  production, the EBD is not necessary to prevent immunopathology.

We hypothesized that the high evolutionary selective pressure for the KRKR motif of IFN $\gamma$  is associated with chronic antigen stimulation, as occurs during infections with delayed pathogen elimination. To test this hypothesis, we infected IFN $\gamma^{\Delta\text{KRKR}}$  and IFN $\gamma^{\text{wt}}$  mice with intermediate doses of LCMV-Docile (Fig. 4b), which induces a self-limiting infection with prolonged immune stimulation due to delayed virus clearance<sup>2</sup>. Starting around 6 d after infection, both IFN $\gamma^{\text{wt}}$  and IFN $\gamma^{\Delta\text{KRKR}}$  mice lost body weight (Fig. 4c). While IFN $\gamma^{\text{wt}}$  mice regained weight and recovered from day 9 onward, IFN $\gamma^{\Delta\text{KRKR}}$  mice continued to lose weight, and 7 of 12 mice had to be killed until day 13 according to endpoint criteria (Fig. 4d). IFN $\gamma^{\Delta\text{KRKR}}$  mice showed strongly reduced peripheral body temperature (Fig. 4e) and increased serum IFN $\gamma$  levels (Fig. 4f). Severe sickness behavior and immunopathology in IFN $\gamma^{\Delta\text{KRKR}}$  mice was evidenced by decreased red blood cell and platelet counts as well as decreased hemoglobin compared to IFN $\gamma^{\text{wt}}$  mice, while white blood cell counts were comparable (Fig. 4g). Compared to IFN $\gamma^{\text{wt}}$  mice, IFN $\gamma^{\Delta\text{KRKR}}$  mice showed strongly increased lactate dehydrogenase (LDH), glutamate–pyruvate transaminase (GPT) and ferritin levels but normal serum triglyceride levels (Fig. 4h). As assessed by histology, some LCMV-infected IFN $\gamma^{\Delta\text{KRKR}}$ , but not IFN $\gamma^{\text{wt}}$ , mice showed areas of necrosis in the liver (Extended Data Fig. 5a), indicating more severe liver damage in IFN $\gamma^{\Delta\text{KRKR}}$  mice. Enhanced toxicity also correlated with reduced liver and spleen weights in IFN $\gamma^{\Delta\text{KRKR}}$  mice (Fig. 4i). No meaningful differences in viral load in liver, spleen, kidney, lung and brain were detected between IFN $\gamma^{\text{wt}}$  and IFN $\gamma^{\Delta\text{KRKR}}$  mice (Extended Data Fig. 5b). In line with the less pronounced splenomegaly, significantly lower spleen cell counts were observed in IFN $\gamma^{\Delta\text{KRKR}}$  mice than in IFN $\gamma^{\text{wt}}$  mice (Extended Data Fig. 6a). No differences between the two mouse groups were observed in the percentages of CD8<sup>+</sup> T cells and the LCMV-specific GP33- or NP396-reactive CD8<sup>+</sup> T cells, while absolute numbers of LCMV-specific GP33- or NP396-reactive CD8<sup>+</sup> T cells were slightly decreased in IFN $\gamma^{\Delta\text{KRKR}}$  mice (Extended Data Fig. 6b–d). The relative sizes of effector subpopulations, namely early effector cells (KLRG-1<sup>-</sup>/CD127<sup>-</sup>), short-lived effector cells (KLRG-1<sup>-</sup>/CD127<sup>-</sup>) and memory precursor effector cells (KLRG-1<sup>-</sup>/CD127<sup>+</sup>), were not affected by IFN $\gamma$  lacking the EBD, but again, absolute numbers of early effector cells and memory precursor effector cells were slightly decreased in IFN $\gamma^{\Delta\text{KRKR}}$  mice (Extended Data Fig. 6e). IFN $\gamma^{\Delta\text{KRKR}}$  mice exhibited lower percentages and absolute numbers of naive CD8<sup>+</sup> T cells and higher percentages but lower absolute numbers of effector memory T cells. Also, lower relative and absolute numbers of CD8<sup>+</sup> T cells with a central memory T cell phenotype were observed in IFN $\gamma^{\Delta\text{KRKR}}$  mice (Extended Data Fig. 6f). Comparable coexpression of inhibitory receptors PD-1

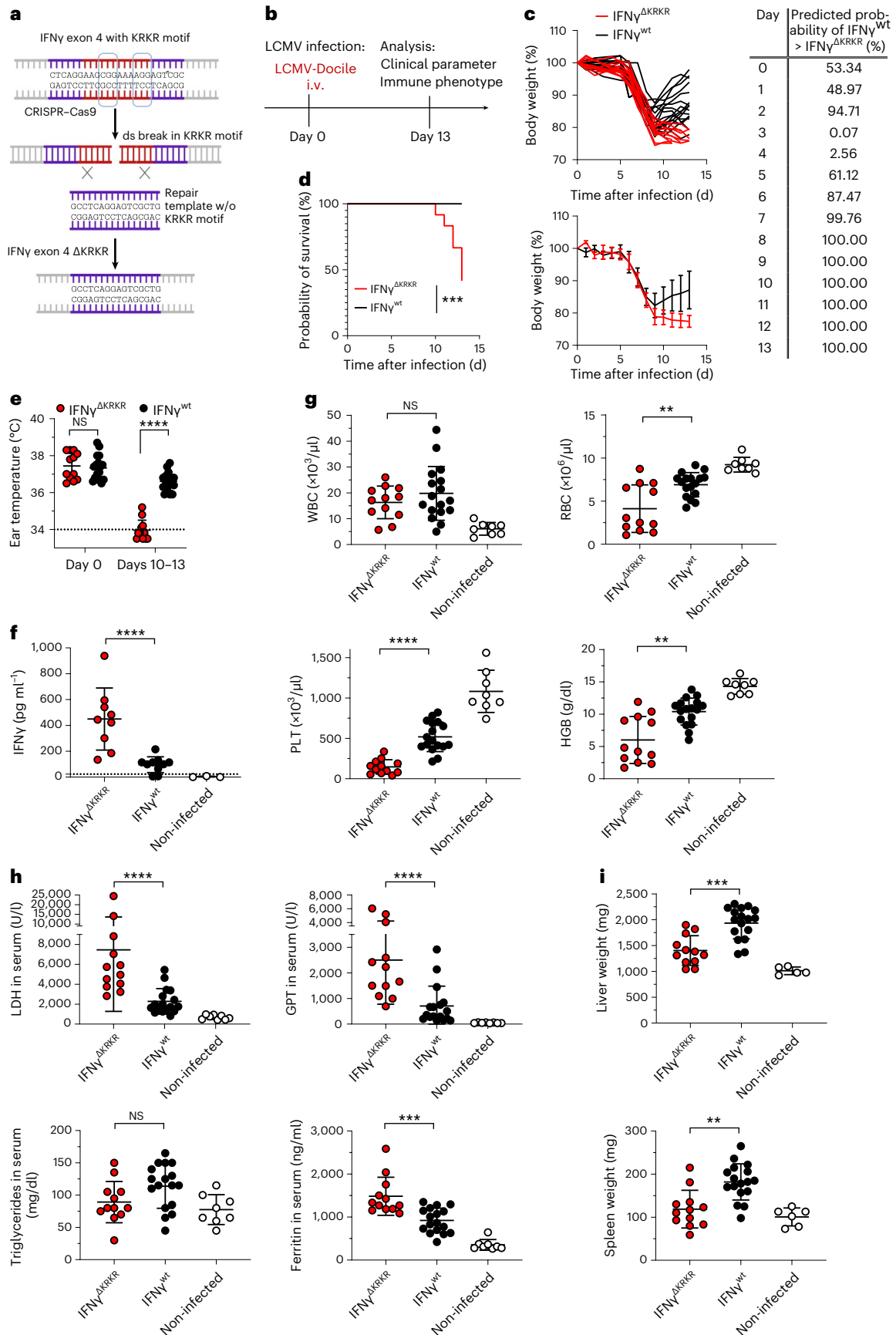


**Fig. 4 | IFN $\gamma^{\text{AKRRR}}$  mice succumb to viral infections.** **a**, CRISPR–Cas9 approach for the generation of IFN $\gamma^{\text{AKRRR}}$  mice; ds, double-strand. **b**, Scheme of IFN $\gamma^{\text{AKRRR}}$  (red) or IFN $\gamma^{\text{WT}}$  (black) mice infected with LCMV-Docile and monitored for 13 d; i.v., intravenous. **c**, Weight curves of IFN $\gamma^{\text{AKRRR}}$  (red) and IFN $\gamma^{\text{WT}}$  (black) mice following infection. IFN $\gamma^{\text{AKRRR}}$  mice deteriorated from days 8 to 9 as determined by weight loss, while IFN $\gamma^{\text{WT}}$  mice recovered. The table shows the predicted probability of the weight of IFN $\gamma^{\text{WT}}$  mice being greater than the weight of IFN $\gamma^{\text{AKRRR}}$  mice in percent. **d**, Survival analysis of mice shown in **c** ( $P = 0.0003$ ). Mice from the IFN $\gamma^{\text{AKRRR}}$  group had to be killed due to increased weight loss starting from day 10. **e**, Ear temperature of IFN $\gamma^{\text{AKRRR}}$  and IFN $\gamma^{\text{WT}}$  mice before and 10–13 d after LCMV infection. **f**, Serum IFN $\gamma$  levels in IFN $\gamma^{\text{AKRRR}}$  and IFN $\gamma^{\text{WT}}$  mice at endpoint analysis. Non-infected mice are shown as controls. **g**, Parameters from the blood analysis of IFN $\gamma^{\text{AKRRR}}$  mice show reduced white blood cell (WBC), red blood cell (RBC;  $P = 0.0077$ ) and platelet (PLT) counts as well as reduced hemoglobin (HGB;  $P = 0.0018$ ) compared to IFN $\gamma^{\text{WT}}$  mice after infection. Non-infected mice

are shown as controls. **h**, Elevated LDH, GPT and ferritin ( $P = 0.0003$ ) levels but similar amounts of triglycerides were detected in the sera of IFN $\gamma^{\text{AKRRR}}$  mice (red) compared to IFN $\gamma^{\text{WT}}$  mice (black). **i**, Liver and spleen pathology in IFN $\gamma^{\text{AKRRR}}$  mice (red) is indicated by reduced organ weight ( $P = 0.0002$  for liver weight and  $P = 0.001$  for splenic weight) after infection compared to IFN $\gamma^{\text{WT}}$  mice (black). Shown are data from 9–17 mice from three to four independent experiments, and data are shown as mean  $\pm$  s.d. Significance was calculated by Mantel–Cox test for survival or Mann–Whitney test (two sided); \*\* $P \leq 0.01$ , \*\*\* $P \leq 0.001$  and \*\*\*\* $P \leq 0.0001$ . For the data in **c**, statistical analyses were performed using a linear mixed model with random intercept for each individual and an interaction effect between time and group, where time was parameterized by restricted cubic splines with four knots to account for non-linearity. From this model, the predictive distribution was computed via bootstrap samples, and the predicted probability of IFN $\gamma^{\text{WT}} >$  IFN $\gamma^{\text{AKRRR}}$  was calculated.

and LAG-3 on CD8 $^+$  T cells was observed, but again, reduced numbers were detectable in IFN $\gamma^{\text{AKRRR}}$  mice (Extended Data Fig. 6g). The percentage of IFN $\gamma$ -expressing CD8 $^+$  T cells was comparable after in vitro restimulation with GP33 peptide and was slightly increased in NP396 peptide-stimulated CD8 $^+$  T cells from IFN $\gamma^{\text{AKRRR}}$  mice; no differences in absolute numbers between both groups were observed (Extended Data Fig. 6h). In summary, differentiation of effector CD8 $^+$  T cells into various subpopulations was largely comparable between IFN $\gamma^{\text{AKRRR}}$  and IFN $\gamma^{\text{WT}}$  mice in the context of LCMV infection with slightly lower absolute numbers of some CD8 $^+$  T cell subpopulations observed in IFN $\gamma^{\text{AKRRR}}$  mice.

To exclude the possibility that the slight decrease in IFN $\gamma^{\text{AKRRR}}$  in the on rate of the binding response to IFN $\gamma$ R1 (detected in the SPR analysis (Fig. 1g)) altered receptor-proximal signaling, as has been described for other mutant IFN $\gamma$  molecules<sup>22</sup>, and thus would have caused the toxicity, we compared signaling properties of both IFN $\gamma^{\text{WT}}$  and IFN $\gamma^{\text{AKRRR}}$  in terms of PD-L1 upregulation and STAT1 phosphorylation. Splenocytes and fibroblasts incubated with IFN $\gamma^{\text{WT}}$  and IFN $\gamma^{\text{AKRRR}}$  upregulated the expression of PD-L1 in a similar fashion (Extended Data Fig. 7) and with similar kinetics and magnitude induced the phosphorylation of STAT1 (Extended Data Fig. 8) in IFN $\gamma$ R-competent, but not IFN $\gamma$ R-deficient, cells. This suggested that the immunopathology was not due to alterations in IFN $\gamma$ R signaling or PD-L1 regulation by IFN $\gamma^{\text{AKRRR}}$ . Because T cell responses and viral load were largely similar and receptor-proximal signaling was not altered by deletion of the EBD, we conclude that the severe clinical phenotype was likely associated with elevated serum IFN $\gamma^{\text{AKRRR}}$  levels, as was also observed in the reductionist tumor model.

## Discussion

We have shown that IFN $\gamma$  binds to HSPG of the ECM in vivo in close proximity to its production and is locally retained for at least 48 h. Binding is mediated by four positively charged amino acids at the C terminus of IFN $\gamma$  interacting with the negatively charged HS. This motif, which in most species is KRKR, is often flanked by additional positively charged amino acids, for example, RKRKR in the koala. In 50 species covering 450 million years of vertebrate evolution, the motif consisting of four positively charged amino acids is conserved. Deviations from the KRKR motif are without exception positively charged amino acids, for example, RRRR in the elephant shark. In human IFN $\gamma$ , the motif occurs twice in the C terminus (KRKR ... RGRR), and in mice, the motif occurs only once (KRKR). Therefore, investigating mouse IFN $\gamma$  was straightforward in this hypothesis-driven approach based on the assumption that evolutionary conservation is a strong indicator for its importance.

The ability of IFN $\gamma$  to bind to HS is well recognized<sup>9</sup>. Five hundred and eighty proteins bind to HS/heparin, and numerous cytokines, chemokines or growth factors contain a motif of several, not necessarily contiguous, positively charged amino acids<sup>23</sup>. It was suggested

that the binding of various proteins to HS plays multiple roles, such as in the regulation of leukocyte development, leukocyte migration, immune activation and inflammatory processes<sup>24</sup>. Most analyses to date were based on in vitro assays. It has been suggested that cell surface HS facilitates binding of IFN $\gamma$  to IFN $\gamma$ R<sup>12</sup> or that the KRKR motif acts as a nuclear localization signal, enhancing the biological activity of IFN $\gamma$ <sup>11</sup>. As IFN $\gamma^{\text{AKRRR}}$  has retained normal biological activity (for example, IFN $\gamma$ R-proximal signaling), these mechanisms appear of minor importance. It was also suggested that local IFN $\gamma$  binding to HS increases its availability<sup>25</sup> or that binding of IFN $\gamma$  to tumor phosphatidylserine converts transient exposure into long-lived inflammation<sup>26</sup>. However, IFN $\gamma^{\text{AKRRR}}$  T cells rejected large tumors as efficiently as IFN $\gamma^{\text{WT}}$  T cells, indicating that local retention of IFN $\gamma$  is not required in a model of IFN $\gamma$ -dependent rejection of established solid tumors. Whether binding of IFN $\gamma^{\text{AKRRR}}$  to phosphatidylserine is retained and plays a role in tumor rejection remains to be determined. Additionally, the pharmacokinetics of IFN $\gamma$  have been analyzed, for example, when bound to heparin, and binding of IFN $\gamma$  to HS may protect the cytokine from degradation and regulate its activity<sup>27,28</sup>. However, IFN $\gamma$ –HS binding has not been implicated as a mechanism to prevent immunopathology, as shown here in two in vivo models in a side-by-side comparison of IFN $\gamma^{\text{WT}}$  and IFN $\gamma^{\text{AKRRR}}$ . In the first model, the local expression of IFN $\gamma^{\text{AKRRR}}$  compared to IFN $\gamma^{\text{WT}}$  in solid tumors resulted in reduced local retention, increased systemic serum levels and wasting disease within a few days. Similarly, in the second model, IFN $\gamma^{\text{AKRRR}}$ , but not IFN $\gamma^{\text{WT}}$ , mice experienced severe immunopathology with increased systemic IFN $\gamma^{\text{AKRRR}}$  levels following LCMV infection. Sequestration seems to be particularly important during infection, with delayed virus clearance and prolonged IFN $\gamma$  production.

Several mechanisms that reduce immunopathology have been described. Regulatory T cells as well as immune checkpoints diminish T cell effector function<sup>2–4</sup>. Pathogens can be tolerated to minimize tissue damage<sup>29</sup>. Finally, previous pathogen exposure can increase the kinetics and magnitude of immune responses to subsequent, even antigen-unrelated, infections, thereby minimizing the risk of immunopathology<sup>30,31</sup>. Mice in the current study were kept under specific pathogen-free (SPF) conditions; therefore, future analysis of mice with a natural, wild microbiome will be of interest<sup>32</sup>. Together, we describe an evolutionarily conserved mechanism to prevent immunopathology by restraining IFN $\gamma$  at its local site of production and avoiding IFN $\gamma$  toxicity from systemic release at high concentrations.

## Online content

Any methods, additional references, Nature Portfolio reporting summaries, source data, extended data, supplementary information, acknowledgements, peer review information; details of author contributions and competing interests; and statements of data and code availability are available at <https://doi.org/10.1038/s41590-023-01420-5>.

## References

- Hedrick, S. M. The acquired immune system: a vantage from beneath. *Immunity* **21**, 607–615 (2004).
- Barber, D. L. et al. Restoring function in exhausted CD8 T cells during chronic viral infection. *Nature* **439**, 682–687 (2006).
- Sakaguchi, S., Fukuma, K., Kuribayashi, K. & Masuda, T. Organ-specific autoimmune diseases induced in mice by elimination of T cell subset. I. Evidence for the active participation of T cells in natural self-tolerance; deficit of a T cell subset as a possible cause of autoimmune disease. *J. Exp. Med.* **161**, 72–87 (1985).
- Tivol, E. A. et al. Loss of CTLA-4 leads to massive lymphoproliferation and fatal multiorgan tissue destruction, revealing a critical negative regulatory role of CTLA-4. *Immunity* **3**, 541–547 (1995).
- Toyonaga, T. et al. Chronic active hepatitis in transgenic mice expressing interferon- $\gamma$  in the liver. *Proc. Natl Acad. Sci. USA* **91**, 614–618 (1994).
- Alexander, W. S. et al. SOCS1 is a critical inhibitor of interferon  $\gamma$  signaling and prevents the potentially fatal neonatal actions of this cytokine. *Cell* **98**, 597–608 (1999).
- Thibaut, R. et al. Bystander IFN- $\gamma$  activity promotes widespread and sustained cytokine signaling altering the tumor microenvironment. *Nat. Cancer* **1**, 302–314 (2020).
- Hoekstra, M. E. et al. Long-distance modulation of bystander tumor cells by CD8<sup>+</sup> T-cell-secreted IFN- $\gamma$ . *Nat. Cancer* **1**, 291–301 (2020).
- Lortat-Jacob, H., Kleinman, H. K. & Grimaud, J. A. High-affinity binding of interferon- $\gamma$  to a basement membrane complex (Matrigel). *J. Clin. Invest.* **87**, 878–883 (1991).
- Dobeli, H. et al. Role of the carboxy-terminal sequence on the biological-activity of human immune interferon (IFN- $\gamma$ ). *J. Biotechnol.* **7**, 199–216 (1988).
- Subramaniam, P. S., Larkin, J. 3rd, Mujtaba, M. G., Walter, M. R. & Johnson, H. M. The COOH-terminal nuclear localization sequence of interferon  $\gamma$  regulates STAT1  $\alpha$  nuclear translocation at an intracellular site. *J. Cell Sci.* **113**, 2771–2781 (2000).
- Sadir, R., Forest, E. & Lortat-Jacob, H. The heparan sulfate binding sequence of interferon- $\gamma$  increased the on rate of the interferon- $\gamma$ -interferon- $\gamma$  receptor complex formation. *J. Biol. Chem.* **273**, 10919–10925 (1998).
- Savan, R., Ravichandran, S., Collins, J. R., Sakai, M. & Young, H. A. Structural conservation of interferon  $\gamma$  among vertebrates. *Cytokine Growth Factor Rev.* **20**, 115–124 (2009).
- Hemmi, S. et al. Cloning of murine interferon  $\gamma$  receptor cDNA: expression in human cells mediates high-affinity binding but is not sufficient to confer sensitivity to murine interferon  $\gamma$ . *Proc. Natl Acad. Sci. USA* **86**, 9901–9905 (1989).
- Kammertoens, T. et al. Tumour ischaemia by interferon- $\gamma$  resembles physiological blood vessel regression. *Nature* **545**, 98–102 (2017).
- Saesen, E. et al. Insights into the mechanism by which interferon- $\gamma$  basic amino acid clusters mediate protein binding to heparan sulfate. *J. Am. Chem. Soc.* **135**, 9384–9390 (2013).
- van der Loos, C. M. et al. Immunohistochemical detection of interferon- $\gamma$ : fake or fact? *J. Histochem. Cytochem.* **49**, 699–710 (2001).
- Tsiantoulas, D. et al. APRIL limits atherosclerosis by binding to heparan sulfate proteoglycans. *Nature* **597**, 92–96 (2021).
- Ferran, C. et al. Inter-mouse strain differences in the in vivo anti-CD3 induced cytokine release. *Clin. Exp. Immunol.* **86**, 537–543 (1991).
- Kohler, J. et al. IFN- $\gamma$  involvement in the severity of Gram-negative infections in mice. *J. Immunol.* **151**, 916–921 (1993).
- Listopad, J. J. et al. Fas expression by tumor stroma is required for cancer eradication. *Proc. Natl Acad. Sci. USA* **110**, 2276–2281 (2013).
- Mendoza, J. L. et al. Structure of the IFN $\gamma$  receptor complex guides design of biased agonists. *Nature* **567**, 56–60 (2019).
- Vallet, S. D., Clerc, O. & Ricard-Blum, S. Glycosaminoglycan-protein interactions: the first draft of the glycosaminoglycan interactome. *J. Histochem. Cytochem.* **69**, 93–104 (2021).
- Simon Davis, D. A. & Parish, C. R. Heparan sulfate: a ubiquitous glycosaminoglycan with multiple roles in immunity. *Front. Immunol.* **4**, 470 (2013).
- Collins, L. E. & Troeberg, L. Heparan sulfate as a regulator of inflammation and immunity. *J. Leukoc. Biol.* **105**, 81–92 (2019).
- Oyler-Yaniv, J. et al. Catch and release of cytokines mediated by tumor phosphatidylserine converts transient exposure into long-lived inflammation. *Mol. Cell* **66**, 635–647 (2017).
- Lortat-Jacob, H., Baltzer, F. & Grimaud, J. A. Heparin decreases the blood clearance of interferon- $\gamma$  and increases its activity by limiting the processing of its carboxyl-terminal sequence. *J. Biol. Chem.* **271**, 16139–16143 (1996).
- Lortat-Jacob, H. & Grimaud, J. A. Interferon- $\gamma$  C-terminal function: new working hypothesis. Heparan sulfate and heparin, new targets for IFN- $\gamma$ , protect, relax the cytokine and regulate its activity. *Cell Mol. Biol.* **37**, 253–260 (1991).
- Medzhitov, R., Schneider, D. S. & Soares, M. P. Disease tolerance as a defense strategy. *Science* **335**, 936–941 (2012).
- Netea, M. G. et al. Trained immunity: a program of innate immune memory in health and disease. *Science* **352**, aaf1098 (2016).
- Niec, R. E., Rudensky, A. Y. & Fuchs, E. Inflammatory adaptation in barrier tissues. *Cell* **184**, 3361–3375 (2021).
- Rosshart, S. P. et al. Laboratory mice born to wild mice have natural microbiota and model human immune responses. *Science* **365**, eaaw4361 (2019).

**Publisher's note** Springer Nature remains neutral with regard to jurisdictional claims in published maps and institutional affiliations.

**Open Access** This article is licensed under a Creative Commons Attribution 4.0 International License, which permits use, sharing, adaptation, distribution and reproduction in any medium or format, as long as you give appropriate credit to the original author(s) and the source, provide a link to the Creative Commons licence, and indicate if changes were made. The images or other third party material in this article are included in the article's Creative Commons licence, unless indicated otherwise in a credit line to the material. If material is not included in the article's Creative Commons licence and your intended use is not permitted by statutory regulation or exceeds the permitted use, you will need to obtain permission directly from the copyright holder. To view a copy of this licence, visit <http://creativecommons.org/licenses/by/4.0/>.

© The Author(s) 2023, corrected publication 2023, 2024

## Methods

### Sequence homology analysis

IFN $\gamma$  protein sequences of different species were compared using FASTA identifiers (Supplementary Table 1) and UniProtKB (<https://www.uniprot.org/uniprot/>). Sequence homology to mouse was determined using sequence alignment via BLAST (accessed on 30 August 2021; <https://blast.ncbi.nlm.nih.gov/Blast.cgi?PAGE=Proteins>).

### Recombinant IFN $\gamma$ variants and SPR

Proteins used for binding studies (Supplementary Table 2) were expressed in *E. coli*. cDNA sequences without the leader peptide were codon optimized and cloned into a pET28-N-His<sub>6</sub>-SUMO vector. IFN $\gamma^{\text{AKRRK}}$  and IFN $\gamma^{\text{AKRRK}}$ -GFP mutants were generated using the QuikChange site-directed mutagenesis kit (Stratagene). The extracellular domain (amino acids 26–254) of the IFN $\gamma$ R1 protein was cloned based on mouse cDNA into a pET26b-N-His<sub>6</sub>-SUMO vector, resulting in periplasmic expression of an N-terminal His<sub>6</sub>-SUMO-tagged protein bearing an additional C-terminal His<sub>6</sub> tag. All proteins were produced using T7 express competent *E. coli* (New England Biolabs) cotransformed with the pRARE plasmid. For purification of IFN $\gamma$  proteins, bacteria were collected and resuspended in lysis buffer (1 $\times$  PBS (pH 7.4), 0.2 M NaCl, 5% glycerol supplemented with cComplete EDTA-free protease inhibitor cocktail (Roche), 0.25% (wt/vol) 3-((3-cholamidopropyl)-dimethylammonio)-1-propanesulfonate, 1 mM phenylmethylsulfonyl fluoride, 100  $\mu$ l of lysozyme (100 mg ml<sup>-1</sup>) and 1  $\mu$ l of benzonase (250 U  $\mu$ l<sup>-1</sup>; Merck) and lysed by two freeze–thaw cycles. Proteins were purified on a HisTrap FF crude column (Cytavia), followed by size-exclusion chromatography on a Superdex 75 column (XK 26  $\times$  60, Cytavia) or Superdex 200 column (XK 26  $\times$  60, Cytavia) for C-terminal GFP fusion proteins, respectively. The N-terminal His<sub>6</sub>-SUMO tag was cleaved with yeast Ulp1p SUMO protease (produced in-house) followed by a gel filtration step and reapplication of the cleaved protein on the Ni<sup>2+</sup> affinity column. For purification of IFN $\gamma$ R1, bacteria were lysed by osmotic shock using 0.2 M Tris-HCl (pH 8.0), 0.5 mM EDTA (pH 8.0), 0.5 M sucrose and 1 mM phenylmethylsulfonyl fluoride as lysis buffer. Purification, as described above, was followed by cleavage of the N-terminal His<sub>6</sub>-SUMO tag and a final gel filtration step on a 10/300 Superdex 200 GL increase column (Cytavia). Recombinant proteins were stored in 20 mM HEPES (pH 7.5) and 0.2 M NaCl at –80 °C until further use. Binding kinetics of IFN $\gamma$  variants to HS and the recombinant IFN $\gamma$ R1 were determined by SPR on a Biacore T200 (GE Healthcare) using a dextran Series S Sensor Chip CM4 (GE Healthcare). For analysis of HS binding, commercial HS derived from porcine intestinal mucosa has been used (Celsus Laboratories), and this preparation was previously characterized<sup>33</sup>. The average molecular weight of HS was determined to be 12 kDa with a polydispersity of 1.59, and its sulfation degree, evaluated by S and N elemental analysis, was –1.4 sulfate groups per disaccharide, on average. For IFN $\gamma$ R1, the Sensor Chip was coated with anti-His<sub>6</sub> (Qiagen), onto which the recombinant IFN $\gamma$ R1 proteins were immobilized.

### pMOV1-T2 vectors for Dox-inducible IFN $\gamma$ variant expression

The pMOV1-T2 vector was used for inducible IFN $\gamma$  expression<sup>15</sup>. Variants with deletion of the KRKR motif ( $\Delta$ KRKR) were generated with the QuikChange Lightning site-directed mutagenesis kit (Agilent) according to manufacturer's instructions. To generate the pMOV1-T2-IFN $\gamma^{\text{AKRRK-IND}}$  vector, the primers 5'-ttgccggaatccagcctcaggagctcgcctgctgagcgg-3' and 5'-tcagcagcgcactcctgagctggattccgg-3' were used to introduce the 12-base pair (bp) deletion. For deletion in the pMOV1-T2-IFN $\gamma^{\text{AKRRK-GFP-IND}}$  vector, the primers 5'-gagagcagcctgaggagcgcctgcccggaggcg-3' and 5'-cgctccgcccagcggctcctcaggctgctcctcggg-3' were used.

### Cell lines

HEK293T cells were cultured in DMEM (GlutaMAX, Gibco, Life Technologies) supplemented with 10% fetal calf serum (heat inactivated; Pan Biotech) and 1 $\times$  antibiotic–antimycotic (Gibco, Life Technologies).

MCA313 is a methylcholanthrene-induced fibrosarcoma cell line derived from IFN $\gamma$ R1-deficient mice<sup>15</sup>, B16-F10 is a melanoma cell line<sup>34</sup>, and 16.113 is a SV40 large T antigen-expressing carcinoma cell line<sup>35</sup>. The latter cells were cultured in RPMI1640 medium (Gibco, Life Technologies) supplemented with 5% fetal calf serum, 1 $\times$  non-essential amino acids, 1 mM sodium pyruvate and 1 $\times$  antibiotic–antimycotic (Gibco, Life Technologies).

### Transduction, cloning and characterization of MCA313 cells

MCA313 cells were transduced using a retroviral vector. Vector particles were produced in HEK293T cells. Transduced cells were cultured, and single cells were sorted to establish cell lines. IFN $\gamma$  variant expression was analyzed by seeding 4  $\times$  10<sup>5</sup> cells in 2 ml per well in a six-well plate and culturing them without or with 10–500 ng ml<sup>-1</sup> Dox for 48 h. IFN $\gamma$  concentration in the supernatant was assessed by enzyme-linked immunosorbent assay (ELISA; BD Biosciences). MCA313 cells harboring IFN $\gamma$ -GFP fusion proteins were analyzed for GFP expression using a MACSQuant 10 (Miltenyi) and FlowJo 10 (BD Biosciences).

### Bioactivity of IFN $\gamma$ variants

The bioactivity of IFN $\gamma$  variants was tested by analyzing MHC class I upregulation on B16-F10 cells. B16-F10 cells (5  $\times$  10<sup>5</sup>) were incubated in RPMI supplemented with supernatants from cells producing the IFN $\gamma$  variants or with proteins produced in *E. coli*. Concentrations of IFN $\gamma$  proteins were determined by ELISA and added to B16-F10 cell cultures in concentrations from 0.001 to 100 ng ml<sup>-1</sup>. After 48 h, B16-F10 cells were stained for MHC class I expression using biotinylated anti-H-2K<sup>b</sup>/H-2D<sup>b</sup> (clone 28-8-6) followed by APC-streptavidin (both BD Biosciences).

To further analyze both IFN $\gamma$  and IFN $\gamma^{\text{AKRRK}}$ , primary splenocytes or immortalized fibroblasts from IFN $\gamma$ R1-deficient or WT C57BL/6 mice were incubated with supernatants from cells producing the two variants. PD-L1 expression and intracellular STAT1 phosphorylation were analyzed by flow cytometry. Cells were acquired on a FACSymphonyA1 and analyzed using FlowJo. For PD-L1 analysis, 1  $\times$  10<sup>6</sup> splenocytes or 5  $\times$  10<sup>4</sup> fibroblasts were incubated in the presence of 10 ng ml<sup>-1</sup> IFN $\gamma$  or IFN $\gamma^{\text{AKRRK}}$ , and after 0 h (untreated) and 24 h, cells were stained with anti-PD-L1 for 30 min (splenocytes were additionally stained for CD4, CD8 and CD19) and analyzed by flow cytometry.

For analysis of STAT1 phosphorylation, the same cells (splenocytes or immortalized fibroblasts) and supernatants were used. Cells were incubated with 50 ng ml<sup>-1</sup> IFN $\gamma$  or IFN $\gamma^{\text{AKRRK}}$  and fixed at 37 °C for 15 min with Fixation Buffer (Biolegend) according to the protocol for intracellular staining of phosphoproteins using True-Phos Perm buffer (Biolegend). Thereafter, cells were permeabilized using True-Phos Perm buffer at –20 °C overnight and stained for 30 min in Cell Staining buffer.

### Mice

Mouse experiments were approved by Landesamt für Gesundheit und Soziales Berlin (G-322/10, G-58/16 and G-114/17) and Regierungspräsidentium Freiburg (G-15/168). In tumor transplantation experiments, the maximum tumor volume allowed was 15  $\times$  15  $\times$  15 mm. This size was never exceeded in the experiments. Mice were randomly assigned into groups when injected with tumor cells. For adoptive T cell therapy (ATT) experiments, mice were allocated to groups based on equal distribution in tumor size between different groups. Investigators were not blinded, as endpoint criteria of mouse experiments were defined before experiments. No data were excluded from analysis. Data sets were acquired prospectively and analyzed in a retrospective manner. Animals used were group housed with two to five mice in individually ventilated cages (Tecniplast, Green Line or Blue Line) and maintained under identical housing conditions, such as a 12-h light/12-h dark cycle (light cycle 6:30 to 18:30), standard pelleted mouse diet (ssniff, article number v1124-300) ad libitum, free access to water, 22  $\pm$  2 °C room temperature and a relative humidity

of  $55 \pm 10\%$ . The cages contained wooden bedding material (Tapvei Estonia, Aspen bedding, 4HK, 10 kg), nestlets (ssniff, H3279-10), a red plastic house (ZOONLAB) and paper tunnels (ZOONLAB, 3084030) as cage enrichment. Animals were handled by male and female caretakers and technicians.

*Rag1*<sup>-/-</sup> (B6.129S7-*Rag1*<sup>tm1Mom</sup>/J, 002216), *Rag2*<sup>-/-</sup> (B6.Cg-*Rag2*<sup>tm1.1Cgn</sup>/J, 008449), TCR-1 (B6.Cg-Tg(TcraY1, TcrbY1)416Tev/J, 005236), C57BL/6N (005304), C57BL/6J (000664), B6.129S7-*Ifng*<sup>tm1Ts</sup>/J (002287) and B6.129S7-*Ifngr1*<sup>tm1Agt</sup>/J (003288) mouse strains were obtained from The Jackson Laboratory. All mice were bred and housed under SPF conditions at the animal facility of the Max-Delbrück-Center. *Ifng*<sup>-/-</sup> *Ifngr1*<sup>-/-</sup> mice were obtained by crossing B6.129S7-*Ifng*<sup>tm1Ts</sup>/J (002287) and B6.129S7-*Ifngr1*<sup>tm1Agt</sup>/J (003288) mice. *Ifng*<sup>-/-</sup> *Ifngr1*<sup>-/-</sup> mice were genotyped by PCR. *Ifng*<sup>-/-</sup> primer specific for the mutant allele (5'-CCTTCTATCGCCTTCTTGACG-3'), a primer for the WT allele (5'-AGAAGTAAGTGAAGGGCCAGAG-3') and a common reverse primer (5'-AGGAAACTGGGAGAGGAGAAATAT-3') were used. *Ifngr1*<sup>-/-</sup> forward primer specific for intron 4 (5'-ATGCAACGGTTCCACC CCC-3'), a reverse primer specific for the introduced neomycin cassette (5'-CCAGTCATAGCCGAATAGCC-3') and a reverse primer specific for intron 5 (5'-CCACCTCAGCACTGTCTTCA-3') were used.

### Antibodies and staining reagents

The antibodies and reagents listed are presented in the following format: (immunogen detected/fluorochrome or conjugate/clone/vendor catalog number/species isotype).

For flow cytometry, the following reagents were used: (CD45.2/APC/104/Biolegend 109814/mouse IgG2a,  $\kappa$ ), (CD3/FITC/145-2C11/BD 553062/Armenian hamster IgG1  $\kappa$ ); (CD45.2/BV421/104/Biolegend 109832/mouse IgG2a,  $\kappa$ ), (CD19 FITC/6D5/Biolegend 115506/rat IgG2a,  $\kappa$ ), (CD11b/BV510/M1/70/Biolegend 101263/rat IgG2b,  $\kappa$ ), (CD11c/FITC/HL3/BD 553801/hamster IgG1), (NK1.1/APC/PK136/Miltenyi 130-117-379/mouse IgG2a), (H-2K<sup>b</sup>/H-2D<sup>b</sup>-biotin/28-8-6/BD 553575/mouse IgG2a,  $\kappa$ ), (staining reagent streptavidin-APC, BD-554067), (CD8/BV421/53-6.7/Biolegend 100753/rat IgG2a,  $\kappa$ ), (Vb7/PE/TR310/BD 553216/rat IgG2b,  $\kappa$ ), (CD3/APC/145-2C11/Biolegend 100312/Armenian hamster IgG), (CD4/APC-Fire750/RM4-4/Biolegend 116019/rat IgG2b,  $\kappa$ ), (CD8/BV510/53-6.7/Biolegend 100751/rat IgG2a,  $\kappa$ ), (KLRG-1/PerCP-Cy5.5/2F1/BD 563595/Syrian hamster IgG2,  $\kappa$ ), (CD127/BV421/A7R34/Biolegend 135023/rat IgG2a,  $\kappa$ ), (CD44/APC/IM7/eBioscience 17-0441-82/rat IgG2b,  $\kappa$ ), (CD62L/BV650/MEL-14/Biolegend 104453/rat IgG2a,  $\kappa$ ), (PD-1/BV785/29F.1A12/Biolegend 135225/rat IgG2a,  $\kappa$ ), (LAG-3/PE-Cy7/C9B7W/Biolegend 125208/rat IgG1  $\kappa$ ), (tetramer custom made: Tet-GP33/PE/Baylor College of Medicine), (tetramer custom made: Tet-NP396/PE/Baylor College of Medicine), (CD45.2/BV711/104/Biolegend 109847/mouse IgG2a,  $\kappa$ ), (CD19/PE/6D5/Biolegend 115508/rat IgG2a,  $\kappa$ ), (CD4/PE-Cy7/RM4-5/Biolegend 116016/rat IgG2a,  $\kappa$ ), (CD8/FITC/53-6.7/Biolegend 100706/rat IgG2a,  $\kappa$ ), (CD3/BV421/145-2C11/Biolegend 100336/Armenian hamster IgG), (CD274/APC/10F.9G2/Biolegend 124312/rat IgG2b,  $\kappa$ ), (Fc block/93/Biolegend 101302/rat IgG2a, I) and (CD4/FITC/RM4-4/Biolegend 100510/rat IgG2a,  $\kappa$ ).

For intracellular cytokine staining, the following reagents were used: (CD8/PerCP-Cy5.5/53-6.7/Biolegend 100733/rat IgG2a,  $\kappa$ ), (CD4/BV650/RM4-4/Biolegend 100545/rat IgG2b,  $\kappa$ ), (IFN $\gamma$ /APC/XMG1.2/Biolegend 505810/rat IgG1  $\kappa$ ), (TNF/FITC/MP6-XT22/Biolegend 506304/rat IgG1  $\kappa$ ), (anti-STAT1/PE/4a/BD 612564/mouse IgG2a) and (isotype control/PE/MOPC-173/BD 558595/mouse IgG2a,  $\kappa$ ).

For histology, the following reagents were used: (HSPG 2/A7L6/Abcam ab2501/rat IgG2a), (goat anti-rat/Alexa 568/Invitrogen A11077), (CD146/Alexa 647/ME-9F1/Biolegend 134702/rat IgG2a,  $\kappa$ ) and (staining reagent: Hoechst 33342/Sigma-Aldrich 14533).

For in vivo applications, the following reagents were used: (CD3/145-2C11/Biolegend 100340/Armenian hamster IgG1  $\kappa$ ) and (Armenian hamster/Biolegend 400940/IgG1  $\kappa$ /isotype control).

### Analysis of HS-IFN $\gamma$ colocalization

To generate samples for histology,  $1 \times 10^6$  MCA313<sup>IFN $\gamma$ -GFP-IND</sup> or MCA313<sup>IFN $\gamma$ ΔKRKR-GFP-IND</sup> cells were injected subcutaneously into the right or left flank of *Ifng*<sup>-/-</sup> *Ifngr1*<sup>-/-</sup> mice at 11–43 weeks of age.

Tumor size was measured, and volumes were determined using the ellipsoid volume formula  $V = \frac{\pi \times a \times b \times c}{6}$ . When tumors reached a size of approximately 300 mm<sup>3</sup> (days 10–12), mice received Dox (1 mg ml<sup>-1</sup> in 2% glucose) via the drinking water for at least 3 d. Thereafter, Dox was removed. Tumors were excised, and sera were taken. One part was fixed in 4% paraformaldehyde (PFA; Sigma-Aldrich) for 24–48 h at 4 °C, followed by an incubation in 30% sucrose in PBS (Gibco) for 24–48 h at 4 °C. Tissue was mounted in optimum cutting temperature compound (Tissue-Tek, Sakura) and frozen at -80 °C.

For colocalization of IFN $\gamma$  and HS, 16- $\mu$ m cryosections of PFA-fixed tissue were stained for HSPG, CD146 and Hoechst. For staining of HS and CD146, antigen retrieval for 6 h at 60 °C with 10 mM citrate buffer (Roth, pH 7.4) was performed. Slides were washed in PBS and blocked in 1% bovine serum albumin (pH 7; Sigma-Aldrich) containing 0.2% Triton X-100 (PanReac AppliChem ITW Reagents) and 0.2% gelatine from coldwater fish (Sigma-Aldrich) for 1 h at room temperature. Slides were washed three times for 5 min each in PBS. HS was visualized using rat anti-HSPG 2 (clone A7L6, Abcam) in antibody diluent (Dako) overnight at 4 °C in the dark. The primary antibody was detected by a goat anti-rat antibody coupled to Alexa 568 (A11077, Invitrogen) incubated for 2 h at room temperature in the dark, followed by simultaneous CD146 and nuclear staining using a directly labeled CD146-Alexa 647 antibody (clone ME-9F1, Biolegend) and Hoechst 33342 (Sigma-Aldrich), incubating for 2 h at room temperature in the dark. Image acquisition and processing of imaging raw data were performed on a Zeiss LSM 980 AiryScan 2 system (Carl Zeiss Microscopy) using the AiryScan MPLX SR-4Y mode with a final pixel size of 0.065  $\mu$ m  $\times$  0.065  $\mu$ m and a z sampling rate of 0.3  $\mu$ m. Images were acquired with a  $\times 20/0.8$ -NA Plan-Apochromat Air objective (working distance of 0.55 mm). Diode laser lines at 639 nm (Alexa 647), 561 nm (Alexa 568), 488 nm (GFP) and 405 nm (Hoechst) were used to excite the fluorophores. To detect the fluorophore emissions, detection wavelengths were set to 659–720 nm (Alexa 647), 574–627 nm (Alexa 568), 499–548 nm (GFP) and 422–477 nm (Hoechst). For each section, six separate positions were defined within one region of the sample. Appropriate areas were chosen by abundance of capillaries. For comparability of the samples, all recordings were performed with the same instrument parameter settings. Thresholds for CD146 and HS were set based on negative controls and were applied globally. Only in rare exceptions was the threshold adjusted manually, again using negative controls. For GFP, the threshold was set based on tissue without Dox induction as negative controls to exclude autofluorescence from the tissue. Sections with necrotic or folded tissue were generally excluded from the analysis. To calculate a colocalization channel between HS and IFN $\gamma$ -GFP or IFN $\gamma$ <sup>ΔKRKR</sup>-GFP, CD146 staining was used to calculate a mask, which was applied to the two channels of interest. By working with masked channels (HS in the basement membrane and GFP), all voxels outside of the CD146 region were set to 0 in these regions and thus excluded from building a colocalization channel. The object-based volumes, which indicate overlapping regions of masked HS and GFP, were calculated from colocalization and were normalized to CD146 volumes to get final values. Segmentation, colocalization analysis and visualization were performed with Imaris version 9.7.2 (Bitplane, Oxford Instruments).

### Detection of IFN $\gamma$

Part of the tumor was used to extract IFN $\gamma$  from the tumor tissue. Tumors were weighed and dissociated in 4 ml of RPMI containing 300  $\mu$ g ml<sup>-1</sup> DNase I (Roche) using a C-tube and a GentleMACS dissociator (Miltenyi). C-tubes were centrifuged at 800g for 10 min, and supernatants were collected. Supernatants were centrifuged at

13,000g for 10 min, collected and stored at  $-80^{\circ}\text{C}$  for analysis. Sera and tumor supernatant were diluted 1:200 and 1:1,000, respectively, and IFN $\gamma$  concentrations were determined using a mouse IFN $\gamma$  ELISA (BD Biosciences).

### Serum half-life of IFN $\gamma$ variants

To determine the serum half-life of IFN $\gamma$  variants, 14- to 30-week-old *Irfng<sup>-/-</sup>Irfngr1<sup>-/-</sup>* mice were injected with MCA313 cells, as described above. Mice received Dox for 3 d when tumors reached approximately 300 mm<sup>3</sup>, then Dox was removed. Serum was collected, and IFN $\gamma$  concentrations were determined by ELISA. Half-life was calculated using a non-linear fit of a one-phase decay model in GraphPad Prism 9.

### Local release of IFN $\gamma$ variants in vivo

Male or female C57BL/6 or Rag2-deficient mice were injected subcutaneously with  $1 \times 10^6$  MCA313<sup>IFN $\gamma$ -IND</sup>, MCA313<sup>IFN $\gamma$ ΔKRKR-IND</sup>, MCA313<sup>IFN $\gamma$ -GFP-IND</sup> or MCA313<sup>IFN $\gamma$ ΔKRKR-GFP-IND</sup> cancer cells into the left or right flank at 7–33 weeks of age (average of 16 weeks). Tumor size was assessed and calculated as described above. Administration of Dox via the drinking water was initiated when tumors reached 500–600 mm<sup>3</sup>. Animal well-being was monitored daily, and weight was determined beginning with Dox administration. In one cohort, temperature on the abdomen was assessed using an infrared thermometer for rodents (Bioseb). Sera and tumor supernatants were collected as described above.

### Generation of IFN $\gamma$ <sup>ΔKRKR</sup> mice using CRISPR–Cas9 gene editing

Knock-in mice lacking the EBD of IFN $\gamma$  (IFN $\gamma$ <sup>ΔKRKR</sup>) were generated using CRISPR–Cas9. gRNAs within the fourth exon of *Irfng* (chromosome 10, NCBI sequence [NC\\_000076.6](https://www.ncbi.nlm.nih.gov/nuccore/NC_000076.6)) were identified using the CRISPOR tool (<http://crispor.tefor.net/>)<sup>36</sup>. Two gRNAs (gRNA 1, 5′-ccagcctcaggaagcg gaaa-3′; gRNA 2, 5′-cggaatccagcctcaggaag-3′) were chosen for targeting the KRKR sequence (agg and cgg). A 120-nucleotide (nt) repair template introducing the targeted 12-bp deletion was provided for homology-directed repair, spanning 60 nt upstream and downstream of the KRKR coding sequence (5′-caagcattcaatgagctcatccgagtggtc caccagctgttgcgggaatccagcctcaggaagtcgctgctgattcgggtggggaagagatt gtcccaataagaataattctgcagcac-3′). Repair template and gRNAs (synthesized by IDT) were electroporated into C57BL/6N zygotes together with Cas9 protein using a Bio-Rad XCell electroporator, as described previously<sup>37</sup>. All offspring mice were genotyped by DNA isolation and PCR (5′-TCCATCTTCACTGACCATGATGT-3′ and 5′-CCAGATACAACC CCGCAATC-3′, 480 nt), followed by digestion with AclI (New England Biolabs) overnight. This allowed for discrimination between heterozygous and homozygous offspring.

### Characterization of IFN $\gamma$ <sup>ΔKRKR</sup> mouse lines

Homozygous IFN $\gamma$ <sup>ΔKRKR</sup>, WT littermates and C57BL/6N (both male and female) mice were characterized at 13–16 weeks of age. Mice were killed, and blood was collected in potassium-EDTA tubes (Sarstedt). Peripheral blood mononuclear cells and splenocytes were stimulated for 24 h with anti-CD3/CD28 Dynabeads (Gibco), and supernatants were frozen at  $-80^{\circ}\text{C}$  until analysis by ELISA. Heart, liver, kidney, lung, spleen, brain, thymus and intestinal tissue were collected, fixed in formalin and embedded in paraffin. Tissue sections were stained with hematoxylin and eosin. Splenocytes were analyzed by flow cytometry.

### Induction of transient IFN $\gamma$ responses

For anti-CD3 stimulation, mice received either 20 μg of anti-CD3 (clone 145-2C11) or the Armenian hamster IgG1, κ isotype (both ultra leaf-purified, Biolegend), in 200 μl of sterile PBS (Gibco) intravenously. LPS (Sigma) was injected intraperitoneally at 5 μg per g body weight in PBS (Gibco) or with PBS alone. Blood was obtained, and body weight and temperature were determined. Serum was collected as described above and stored at  $-80^{\circ}\text{C}$  until analysis by IFN $\gamma$  ELISA (BD Bioscience).

### ATT

IFN $\gamma$ <sup>ΔKRKR</sup> mice were bred to TCR-I mice (B6.Cg-Tg(TcraY1,TcrbY1) 416Tev/J, 005236). TCR-I mice are transgenic for a TCR specific for epitope I of SV40 large T. For ATT experiments, female *Rag1<sup>-/-</sup>* mice were injected subcutaneously with  $1 \times 10^6$  16.113 cells. When tumors reached 500–600 mm<sup>3</sup> in size, mice were treated with  $1 \times 10^6$  to  $2 \times 10^6$  TCR-I IFN $\gamma$  or IFN $\gamma$ <sup>ΔKRKR</sup> T cells that were collected from TCR-I/IFN $\gamma$ <sup>ΔKRKR</sup> or TCR-I/IFN $\gamma$ <sup>WT</sup> mice. During ATT, weight and well-being were monitored from the day of transfer. Levels of serum IFN $\gamma$  were determined using a mouse IFN $\gamma$  ELISA (BD Biosciences). T cell expansion was monitored using anti-CD3-APC (clone 145-2C11, Biolegend), anti-CD8-BV421 (clone 53-6.7, Biolegend) and anti- $\nu\beta$ 7-PE (clone TR310, BD Biosciences).

### LCMV experiments

Mouse experiments were approved by Regierungspräsidium Freiburg (G-15/168). Male IFN $\gamma$ <sup>ΔKRKR</sup> mice, WT control littermates and C57BL/6 mice (Janvier; maintained under SPF conditions) were infected intravenously with  $1.5 \times 10^3$  to  $3.0 \times 10^3$  plaque-forming units of LCMV-Docile. Mice were killed if they lost >25% of their body weight or if they showed apathy or neurological failures. From day 5 onward, mice were monitored daily for body weight. Endpoint analysis was done between days 10 and 13 after infection, and clinical and biochemical parameters, such as ear temperature (ThermoScan 6022, BRAUN), blood cell counts (Sysmex KX-21 hematology analyzer), GPT, LDH, triglycerides and ferritin (Roche Modular Analytics Evo), were assessed. IFN $\gamma$  levels in sera were determined by ELISA (Biolegend). LCMV titers in organ homogenates were quantified using a focus-forming assay<sup>38</sup>. For flow cytometry, splenocytes were stained with antibodies for  $\geq 30$  min at  $4^{\circ}\text{C}$ . GP33-specific and NP396-specific CD8<sup>+</sup> T cells were detected with PE-labeled H-2D<sup>b</sup> tetramers from the Tetramer Core Facility at Baylor College of Medicine. For detection of intracellular cytokines,  $10^6$  lymphocytes were stimulated with  $10^{-7}$  M GP33 or NP396 peptide for 4 h, followed by surface staining and intracellular staining for IFN $\gamma$  using a Cytofix/Cytoperm kit (BD Bioscience). Analyses were performed using an LSR Fortessa cytometer (BD Biosciences) and FlowJo software v8.8.7/v10.

Histopathological analysis of mice infected with LCMV-Docile was performed at the endpoint (days 10–13 after infection), and organs (liver, lung, brain, spleen and kidney) were taken, fixed in 4% buffered formalin and embedded in paraffin. Sections were stained with hematoxylin and eosin and analyzed by a veterinary pathologist.

### Software

Data analysis and plotting was performed using Microsoft Excel 2016 and 2019 or GraphPad Prism 9. Statistics were calculated using GraphPad Prism 9 or R software (version 4.1.2). Flow cytometry data were acquired using BD Diva or MACSQuantify and analyzed using FlowJo 10. Sequence analysis and cloning procedures were planned in SnapGene 5. Figure layouts were designed using Adobe Illustrator 2021 and Adobe InDesign 2021 as well as [Biorender.com](https://biorender.com).

### Reporting summary

Further information on research design is available in the Nature Portfolio Reporting Summary linked to this article.

### Data availability

All data generated during this study are available in the article and supplementary files or from the corresponding author upon reasonable request. Source data are provided with this paper.

### References

- Jasnin, M. et al. Dynamics of heparan sulfate explored by neutron scattering. *Phys. Chem. Chem. Phys.* **12**, 3360–3362 (2010).
- Fidler, I. J. Selection of successive tumour lines for metastasis. *Nat. New Biol.* **242**, 148–149 (1973).

35. Willimsky, G. & Blankenstein, T. Sporadic immunogenic tumours avoid destruction by inducing T-cell tolerance. *Nature* **437**, 141–146 (2005).
36. Haeussler, M. et al. Evaluation of off-target and on-target scoring algorithms and integration into the guide RNA selection tool CRISPOR. *Genome Biol.* **17**, 148 (2016).
37. Chen, S. et al. Highly efficient mouse genome editing by CRISPR ribonucleoprotein electroporation of zygotes. *J. Biol. Chem.* **291**, 14457–14467 (2016).
38. Battegay, M. et al. Quantification of lymphocytic choriomeningitis virus with an immunological focus assay in 24- or 96-well plates. *J. Virol. Methods* **33**, 191–198 (1991).

## Acknowledgements

We thank C. Friese and S. Vucikuja for technical assistance and T. Schüler and O. Daumke for discussion. This work was supported by grants from the Wilhelm Sander Stiftung (2020.066.1; T.B. and T.K.), from the European Union (ERC Advanced Grant 882963; T.B.) and from the Deutsche Forschungsgemeinschaft SFB1160 A07 and B04 (P.A.) and SFB TR36 (T.B. and T.K.). This work also used the platforms of the Grenoble Instruct Centre (ISBG; UMS 3518 CNRS-CEA-UJF-EMBL) with support from French Infrastructure for Integrated Structural Biology (ANR-10-INSB-05-02) and Grenoble Alliance for Integrated Structural Cell Biology (ANR-10-LABX-49-01) within the Grenoble Partnership for Structural Biology.

## Author contributions

T.B., T.K., J.K. and P.A. conceived the study, analyzed and interpreted the data and wrote the manuscript. J.K. performed in vitro experiments, SPR experiments (together with E.G. and H.L.-J.), tumor experiments and immune stimulation experiments. P.A., L.D., J.L., S.A.

and K.W. performed LCMV infection experiments and analyzed and interpreted the LCMV data. R. Kühn and J.K. generated the transgenic mice. M.R., C.M. and A.Spo. performed microscopy and analyzed data. R. Klopffleisch performed pathological analysis. D.Z. performed statistical analysis. A.Sch. designed and performed production of purified recombinant proteins.

## Funding

Open access funding provided by Max-Delbrück-Centrum für Molekulare Medizin in der Helmholtz-Gemeinschaft (MDC).

## Competing interests

The authors declare no competing interests.

## Additional information

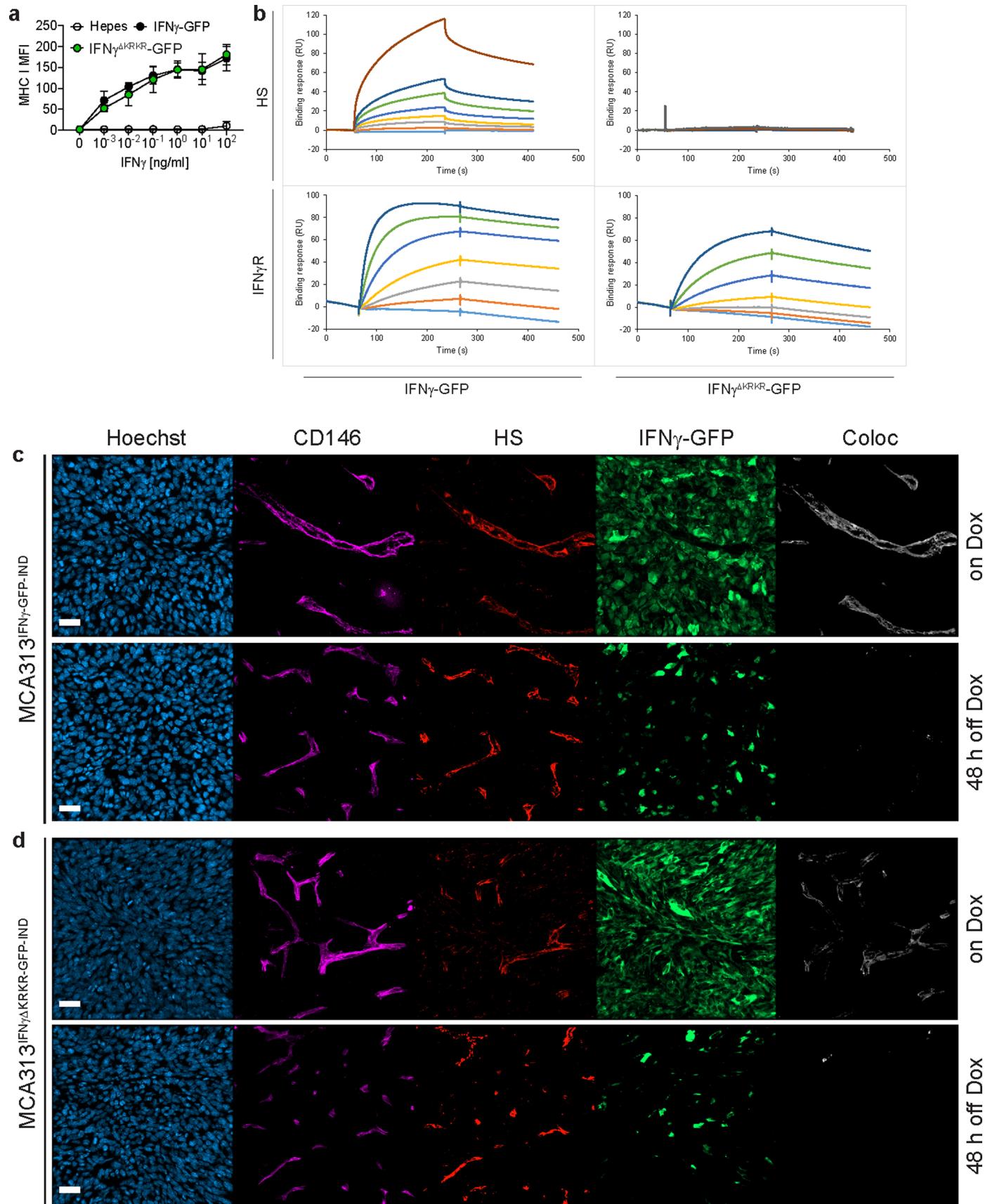
**Extended data** is available for this paper at <https://doi.org/10.1038/s41590-023-01420-5>.

**Supplementary information** The online version contains supplementary material available at <https://doi.org/10.1038/s41590-023-01420-5>.

**Correspondence and requests for materials** should be addressed to Thomas Blankenstein.

**Peer review information** *Nature Immunology* thanks Jeffrey Esko and the other, anonymous, reviewer(s) for their contribution to the peer review of this work. Primary Handling Editor: N. Bernard, in collaboration with the *Nature Immunology* team.

**Reprints and permissions information** is available at [www.nature.com/reprints](http://www.nature.com/reprints).

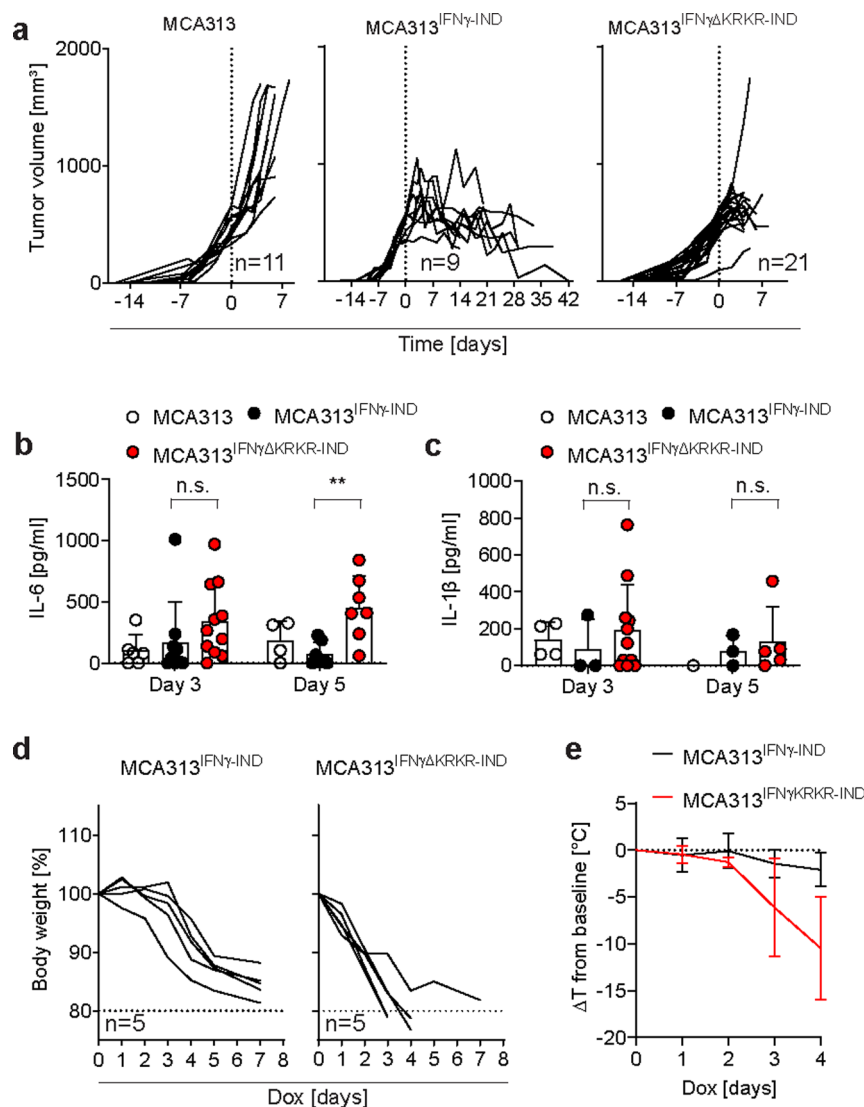


Extended Data Fig. 1 | See next page for caption.

**Extended Data Fig. 1 | IFN $\gamma^{\Delta\text{KRKR}}$ -GFP binds to the IFN $\gamma$ R, but not HS.**

**a**, Upregulation of MHC I on B16-F10 cells by different recombinantly produced IFN $\gamma$ -GFP variants. B16-F10 cells were cultured with the indicated IFN $\gamma$  variant for 48 h or Hepes as control. Shown are means  $\pm$  s.d. of two individual biological experiments. **b**, IFN $\gamma^{\Delta\text{KRKR}}$ -GFP binds to immobilized IFN $\gamma$ R1, but binding to HS is abrogated. IFN $\gamma$ -GFP (upper and lower left panel) or IFN $\gamma^{\Delta\text{KRKR}}$ -GFP (upper and lower right panel) were injected over a HS-activated surface (upper row) or a IFN $\gamma$ R1-activated surface (lower row) during 180 seconds, and the binding response in resonance units (RU) was recorded as a function of time. Each set of sensorgrams was obtained with IFN $\gamma$ -GFP at (from bottom to top): 0, 25, 50, 75,

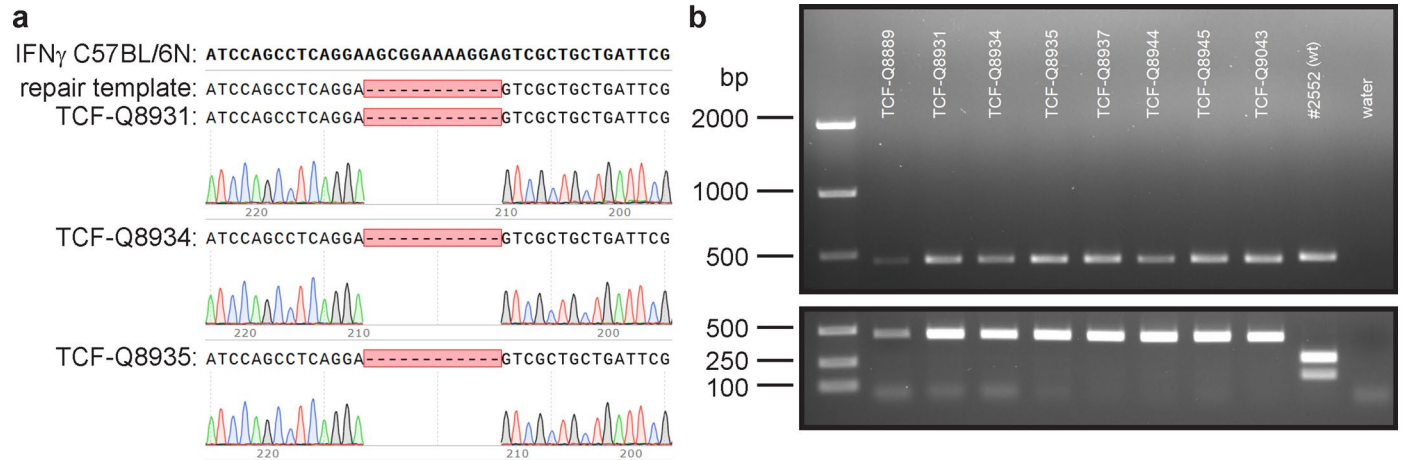
100, 150, 200 and 500 nM for the HS surface and: 0, 1, 2.5, 5, 10, 25 and 50 nM for the IFN $\gamma$ R1 surface. **c, d**, IFN $\gamma^{\prime}$ /IFN $\gamma$ R $^{\prime}$  mice were injected with either MCA313<sup>IFN $\gamma$ -GFP-IND</sup> (c) or MCA313<sup>IFN $\gamma^{\Delta\text{KRKR}}$ -GFP-IND</sup> cells (d). Dox was administered via the drinking water (on Dox) when tumors reached 200-300 mm<sup>3</sup>. Tumors were induced for a minimum of 3 days and then Dox was withdrawn (48 h off Dox). Tumor tissue was stained for CD146, HS and nuclei (Hoechst). Representative confocal images from 2 experiments per time point are shown. Scale bars indicate 30  $\mu$ m. Related data of the same samples are shown in Fig. 2c, d and Extended Data Movie 1.



**Extended Data Fig. 2 | Locally produced IFN $\gamma$ <sup>AKRKR</sup> increases serum levels of IL-1 $\beta$  and IL-6 and causes systemic toxicity in the absence of T cells.**

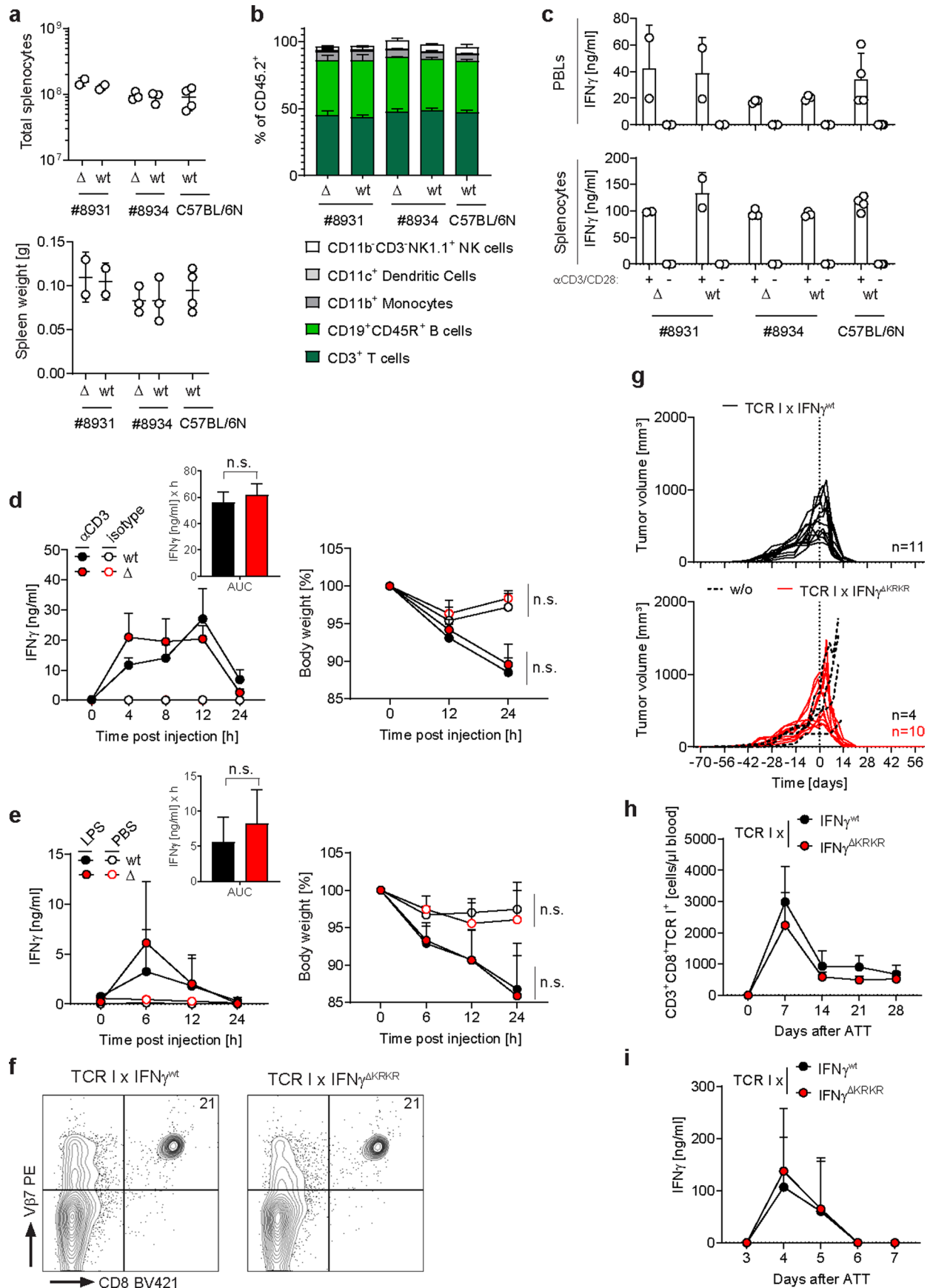
**a**, C57Bl/6 mice harboring MCA313, MCA313<sup>IFN $\gamma$</sup> -IND or MCA313<sup>IFN $\gamma$ AKRKR</sup>-IND tumors received Dox in the drinking water starting at a tumor volume of  $487 \pm 110$  mm<sup>3</sup>,  $487 \pm 95$  mm<sup>3</sup> and  $516 \pm 119$  mm<sup>3</sup>, respectively, as indicated by the dashed vertical line. **b**, IL-6 in the serum of mice on day 3 (left, MCA313 (white circles, n = 6), MCA313<sup>IFN $\gamma$</sup> -IND (black circles, n = 9) or MCA313<sup>IFN $\gamma$ AKRKR</sup>-IND tumors (red circles, n = 11)) and day 5 (right, MCA313 (white circles, n = 4), MCA313<sup>IFN $\gamma$</sup> -IND (black circles, n = 7) or MCA313<sup>IFN $\gamma$ AKRKR</sup>-IND tumors (red circles, n = 7, p = 0.0041)). Individual mice, mean and s.d. are shown. **c**, IL-1 $\beta$  in the serum of mice on day 3 (left, MCA313 (white circles, n = 4), MCA313<sup>IFN $\gamma$</sup> -IND (black circles, n = 3) or MCA313<sup>IFN $\gamma$ AKRKR</sup>-IND (red circles, n = 11)) and day 5 (right, MCA313 (white circles, n = 1), MCA313<sup>IFN $\gamma$</sup> -IND (black

circles, n = 3) or MCA313<sup>IFN $\gamma$ AKRKR</sup>-IND tumors (red circles, n = 5)). Individual mice, mean and s.d. are shown. **d**, **e**, Rag2-deficient mice bearing either MCA313<sup>IFN $\gamma$</sup> -IND or MCA313<sup>IFN $\gamma$ AKRKR</sup>-IND tumors received Dox in the drinking water starting at a tumor volume of  $539 \pm 98$  mm<sup>3</sup> and  $449 \pm 98$  mm<sup>3</sup>, respectively. **d**, weight loss as well as **e**, body temperature (mean  $\pm$  s.d.) was monitored for one week after Dox induction. Data from 1 experiment with n = 5 mice per group is shown. Significance was calculated for **b** and **c**, using the Mann-Whitney test (two-sided) with n.s. not significant, \*\* p  $\leq$  0.01, and for **d**, differences between MCA313<sup>IFN $\gamma$</sup> -IND and MCA313<sup>IFN $\gamma$ AKRKR</sup>-IND tumor bearing mice were analyzed between days 1 and 4 after Dox induction using a linear mixed effects model revealing a strong and increasing difference in weight (p = 0.006 on day 1, p < 0.001 on days 2-4, p-values are adjusted for multiple comparisons by Holm method).



**Extended Data Fig. 3 | Generation of IFN $\gamma$ <sup>ΔKRKR</sup> mice. a**, A PCR fragment of exon 4 of IFN $\gamma$  from CRISPR/Cas9-modified founder mice was sequenced. Sequences were aligned to the native IFN $\gamma$  sequence (C57BL/6 N, NC\_000076.6) and the repair template to validate deletion events. Three out of nine mice are shown. **b**, The deletion of an AcilI restriction site within the KRKR motif indicates zygosity

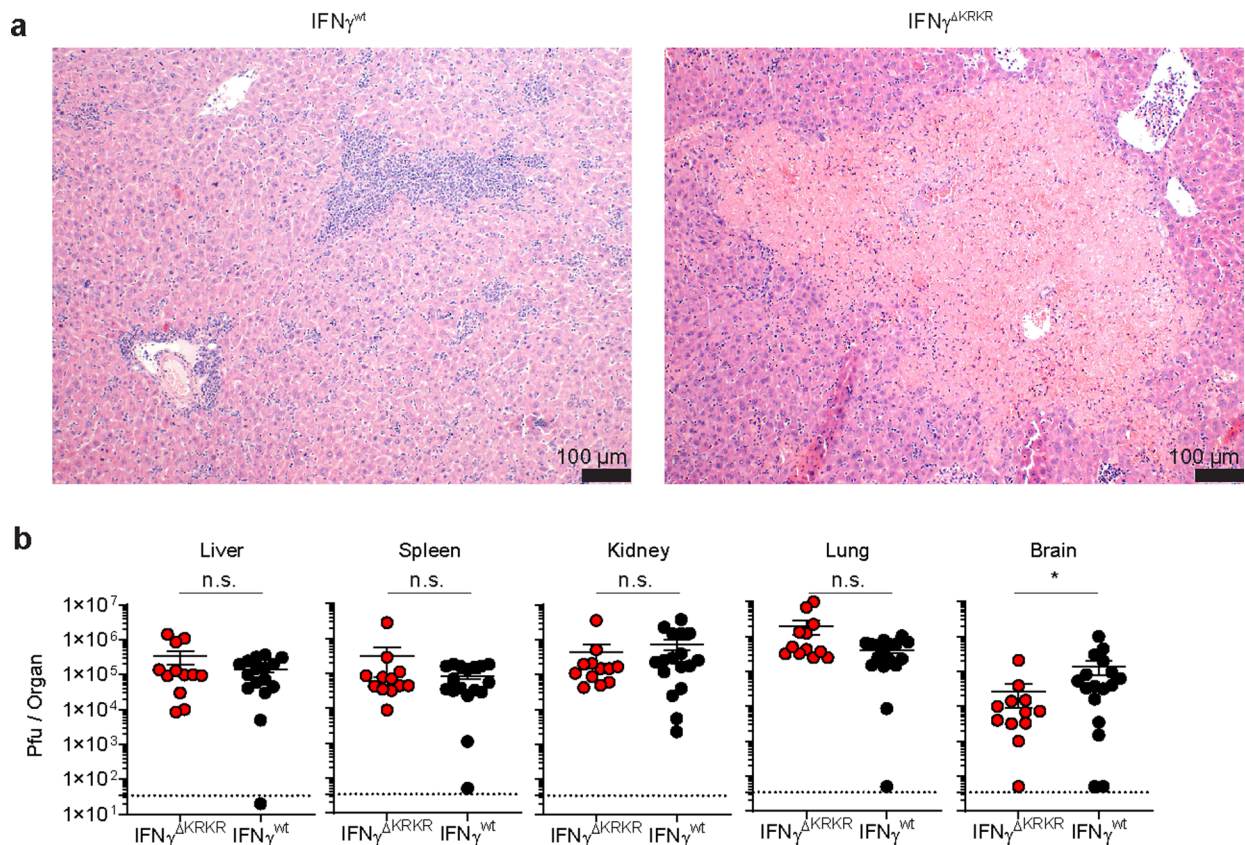
in founder mice. Upper panel shows PCR product, lower panel AcilI digestion. The 480 bp fragment indicates homozygous deletion of 12 bp encoding the KRKR motif. Each lane corresponds to one founder, each founder was genotyped at least twice. The C57BL/6 N mouse #2552 was used as a wild type control (wt).



Extended Data Fig. 4 | See next page for caption.

**Extended Data Fig. 4 | Anti-CD3 antibody treatment, LPS treatment and tumor rejection induce transient IFN $\gamma$  production and no immunopathology in IFN $\gamma^{\Delta\text{KRKR}}$  mice.** **a** Total splenocytes, splenic weight, and **b** splenocyte populations as determined by flow cytometry in IFN $\gamma^{\Delta\text{KRKR}}$  ( $\Delta/\Delta$ ), IFN $\gamma^{\text{WT}}$  (wt/wt) control littermates of two IFN $\gamma^{\Delta\text{KRKR}}$  mouse lines and C57Bl6/N mice. IFN $\gamma^{\Delta\text{KRKR}}$  mice from 1 and C57Bl/6 N mice from 2 experiments are shown. Individual mice, mean and s.d. are shown. **c**, IFN $\gamma$  secretion by CD3/CD28 stimulation of PBL (upper panel) and splenocytes (lower panel) of IFN $\gamma^{\Delta\text{KRKR}}$  and IFN $\gamma^{\text{WT}}$  control littermate of two IFN $\gamma^{\Delta\text{KRKR}}$  lines and C57Bl/6 N mice. Individual IFN $\gamma^{\Delta\text{KRKR}}$  mice from 1 and individual C57Bl/6 N mice from 2 experiments are shown. **d**, Serum IFN $\gamma$  levels (left panel) and relative body weight (right panel) in IFN $\gamma^{\Delta\text{KRKR}}$  ( $n = 5$ , red circles) and wild type control littermates (IFN $\gamma^{\text{WT}}$ ,  $n = 5$ , black circles) after i.v. administration of 20  $\mu\text{g}$  anti-CD3 antibodies. Control mice (IFN $\gamma^{\Delta\text{KRKR}}$   $n = 3$ , IFN $\gamma^{\text{WT}}$   $n = 3$ ) received isotype antibodies. Shown are mean and s.d.. Inlay shows Area under Curve (AUC  $\pm$  SEM) of serum IFN $\gamma$  level through the observed time to depict total secreted IFN $\gamma$  over 24 h. **e**, Serum IFN $\gamma$  level (left panel, mean and s.d.) and AUC  $\pm$  SEM of serum level (inlay) and relative body weight (right panel, mean and s.d.) in IFN $\gamma^{\Delta\text{KRKR}}$  ( $n = 7$ , red circles) and wild type control littermates (IFN $\gamma^{\text{WT}}$ ,  $n = 3$ , black circles) after i.p. administration of 5  $\mu\text{g}/\text{g}$  body weight of LPS. Control mice (IFN $\gamma^{\Delta\text{KRKR}}$   $n = 4$ , IFN $\gamma^{\text{WT}}$   $n = 2$ ) received PBS i.v. IFN $\gamma^{\Delta\text{KRKR}}$  mice from 2 experiments (control littermates only one experiment) are shown.

**f**, Representative flow cytometry plots from two experiments of splenocytes from TCR-1 $\times$  IFN $\gamma^{\Delta\text{KRKR}}$  mice, analyzed on the day of transfer. Splenocytes were stained for CD8 and V $\beta$ 7 antibodies to determine proportion of CD8 $^+$ V $\beta$ 7 $^+$  T cells per spleen. **g**, Rag1 $^{-/-}$  mice were treated with  $1-2 \times 10^6$  TCR-1 $^+$  splenocytes from TCR-1 $\times$  IFN $\gamma^{\text{WT}}$  donor mice (black lines,  $n = 11$ ) or TCR-1 $\times$  IFN $\gamma^{\Delta\text{KRKR}}$  donor mice (red lines, right,  $n = 10$ ) or left untreated (dashed lines, right,  $n = 4$ ) when 16.113 tumors reached 500  $\text{mm}^3$  in size, indicated by the dashed vertical line. Tumor size was monitored for up to 60 days after transfer. **h**, Numbers of CD3 $^+$ CD8 $^+$ TCR-1 $^+$ IFN $\gamma^{\text{WT}}$  (black circles) and CD3 $^+$ CD8 $^+$ TCR-1 $^+$ IFN $\gamma^{\Delta\text{KRKR}}$  (red circles) T cells in the blood of mice in **g** were analysed by flow cytometry over time (shown as mean and s.d.). **i**, Serum from mice in **g** was collected daily from day 3 to day 7 after T cell transfer. IFN $\gamma$  serum levels are shown as mean and s.d.. Significance was calculated using unpaired two-sided t-test for AUC analysis (d,e) with n.s. not significant. For weight in d,e, significance was calculated by contrast tests following a linear mixed model with random intercept for each individual and an interaction effect between time and group. For tumor volume, a linear mixed model was fitted with random intercept for each individual and an interaction effect between time and group, where time was parameterized by restricted cubic splines with 5 knots to account for non-linearity, and from this model the predictive distribution was computed via bootstrap samples and the predicted probability of IFN $\gamma^{\Delta\text{KRKR}} >$  IFN $\gamma^{\text{WT}}$  was calculated.



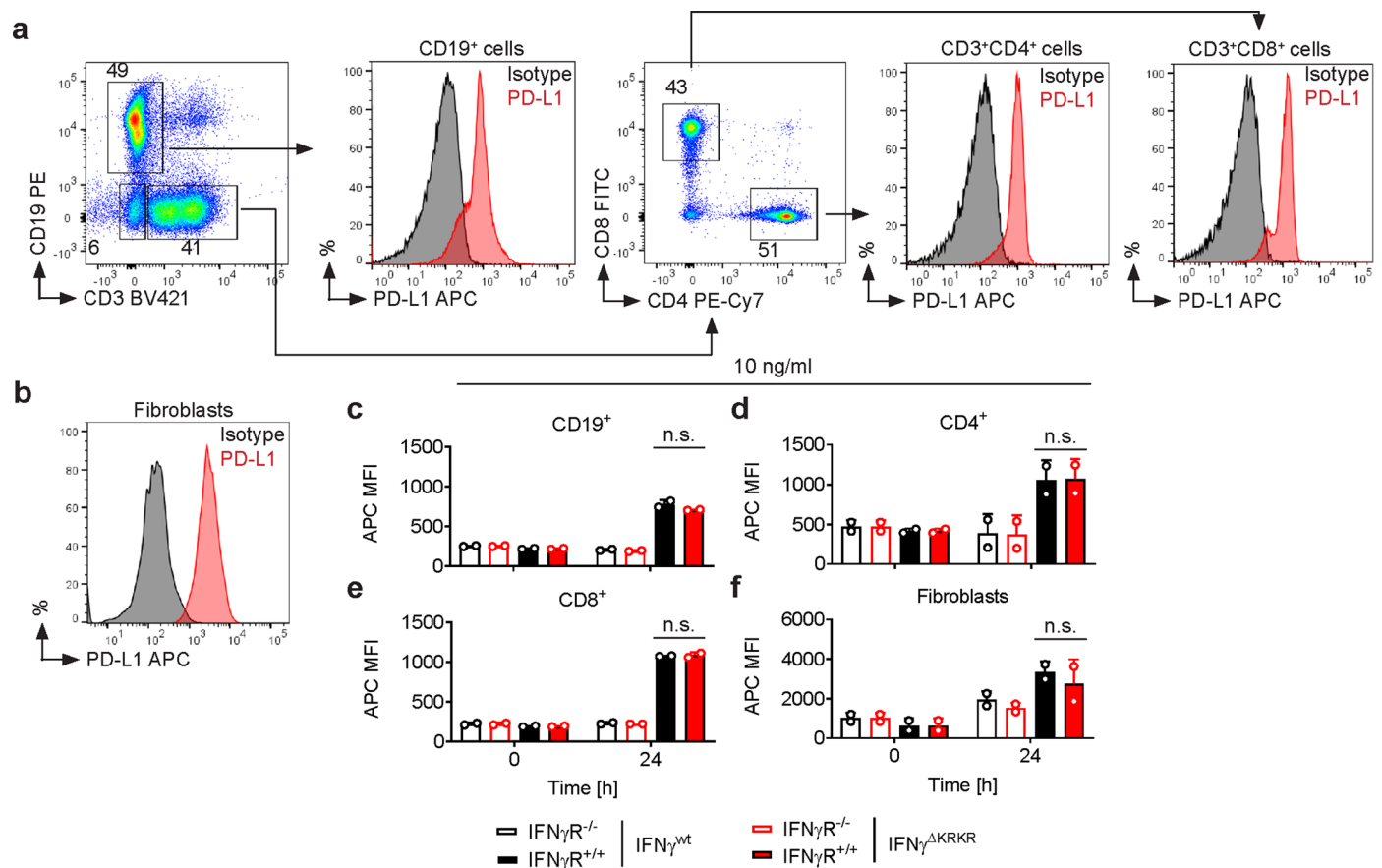
**Extended Data Fig. 5 | Liver necrosis in IFN $\gamma$  <sup>$\Delta$ KRKR</sup> mice and similar virus titers in organs of LCMV-infected IFN $\gamma$  <sup>$\Delta$ KRKR</sup> and IFN $\gamma$ <sup>wt</sup> mice.** Histopathological analysis of organs (liver, kidney, brain, spleen and lung) was performed at the endpoint of LCMV infection experiments (day 10 to 13). **a**, Shown are H&E from liver tissue. Analysis of two independent experiments revealed that 0/5 wildtype littermates and 2/6 IFN $\gamma$  <sup>$\Delta$ KRKR</sup> mice showed massive liver necrosis. **b**, Virus

titers in organs of IFN $\gamma$  <sup>$\Delta$ KRKR</sup> mice (n = 12) and IFN $\gamma$ <sup>wt</sup> control littermate (n = 17) were determined between day 10-13. LCMV-DOCILE was detected in all organs analysed and no meaningful difference was observed between IFN $\gamma$  <sup>$\Delta$ KRKR</sup> and IFN $\gamma$ <sup>wt</sup> mice. Combined results from four experiments (mean  $\pm$  s.e.m.) are shown. Significance was calculated using the two-sided Mann-Whitney test with n.s. not significant, \* p = 0.038.



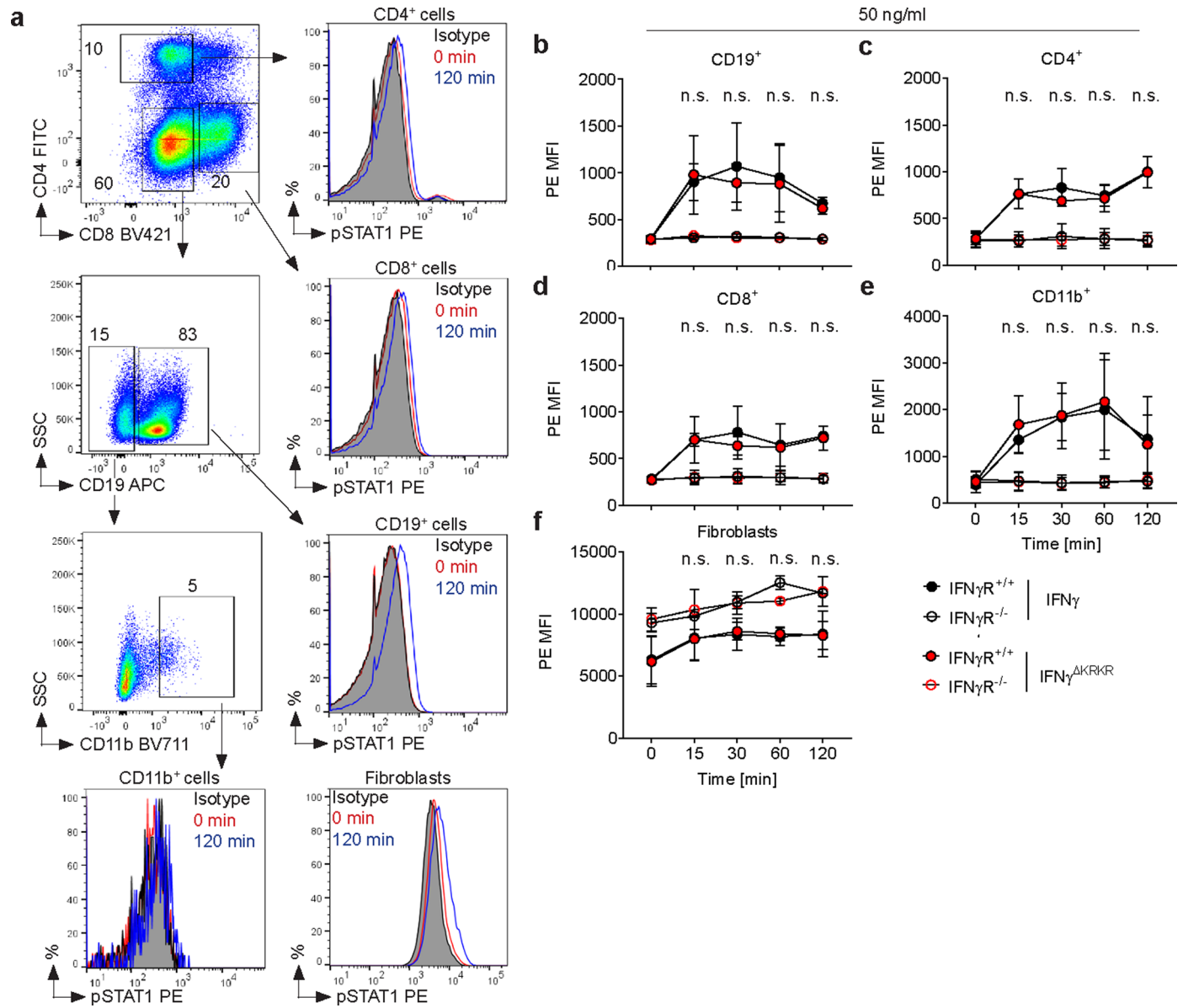
**Extended Data Fig. 6 | Phenotype of CD8 T cells in IFN $\gamma$ <sup>AKRRK</sup> mice after LCMV infection.** IFN $\gamma$ <sup>AKRRK</sup> and IFN $\gamma$ <sup>wt</sup> mice were infected i.v. with LCMV-Docile and analysed between day 10-13. **a**, splenocyte counts and **b**, CD8 T cells within splenocytes. **c**, GP33-specific cells within CD8 T cells. **d**, NP396-specific cells within CD8 T cells. **e**, Differentiation of effector CD8 T cells according to their expression of KLRG-1 and CD127 (exemplary staining shown in the upper two panels) into “EECs” (early effector cells), “SLECs” (short lived effector cells) and “MPECs” (memory precursor effector cells) was followed. **f**, Based on CD62L and CD44 expression (exemplary staining shown in the upper two panels), naïve CD8 T cells were discriminated from effector cells with a T<sub>cm</sub> (central memory)

or T<sub>em</sub> (effector memory) phenotype. **g**, PD-1 and LAG3 expression (exemplary staining shown in the upper two panels) of CD8 T cells after in vitro restimulation with GP33 or NP396 peptides. **h**, IFN $\gamma$  expression (exemplary staining shown in the upper two panels) of CD8 T cells after in vitro restimulation with GP33 or NP396 peptides. In b-h, always relative frequencies (%) as well as absolute cell numbers (#) are shown as individual mice, mean and s.d.. IFN $\gamma$ <sup>AKRRK</sup> (n = 11) and IFN $\gamma$ <sup>wt</sup> (n = 17) mice from four independent experiments are shown. Significance in a-h was calculated using the Mann-Whitney test (two-sided) with n.s. not significant, \* p ≤ 0.05, \*\* p ≤ 0.01, \*\*\* p ≤ 0.001.



**Extended Data Fig. 7 | Similar upregulation of PD-L1 by  $IFN\gamma$  and  $IFN\gamma^{AKRKR}$ .** Splenocytes or fibroblasts were cultured in the presence of 10 ng/ml  $IFN\gamma$  or  $IFN\gamma^{AKRKR}$ . Cells were analyzed 24 h after cytokine exposure for PD-L1 expression. **a**, Gating strategy for splenocytes, and **b**, Example staining of fibroblasts cultured with  $IFN\gamma$ . **c**, CD19<sup>+</sup>; **d**, CD4<sup>+</sup>; **e**, CD8<sup>+</sup>; and **f**, fibroblasts are shown.

Bar diagrams show MFI of PD-L1 staining from two independent biological experiments (mean  $\pm$  s.d.). Comparing average MFI of cells cultured for 24 h with either  $IFN\gamma$  or  $IFN\gamma^{AKRKR}$  using an unpaired t-test revealed no significant differences (n.s.).



**Extended Data Fig. 8 | Similar induction of Stat1 by IFN $\gamma$  and IFN $\gamma$ <sup>AKRKR</sup>.** Splenocytes or fibroblasts were cultured in 50 ng/ml IFN $\gamma$  or IFN $\gamma$ <sup>AKRKR</sup>. **a**, Splenocytes or fibroblasts were analyzed at different time points after cytokine exposure for phospho-Stat1 induction in vitro by flow cytometry. **b**, CD19; **c**, CD4; **d**, CD8; **e**, CD11b; and **f**, fibroblasts are shown. Curve graphs show kinetics

of MFI changes of anti-phospho-Stat1 staining. Shown are mean  $\pm$  s.d. values from 2 (b,c,d,f) or 3 (e) independent biological experiments. Comparing average MFI of cells cultured with either IFN $\gamma$  or IFN $\gamma$ <sup>AKRKR</sup> using a paired two-sided t-test revealed no significant (n.s.) differences for any of the time points analyzed (15, 30, 60, 120 min).

Extended Data Table 1 | Sequence comparison of vertebrate IFN $\gamma$ 

Organism	Motif sequence	Identity to mouse IFN $\gamma$ (%)	Common name	Taxon
<i>Mus musculus</i>	<u>R</u> <u>K</u> <u>R</u> <u>K</u> <u>R</u> <u>R</u> <u>S</u>	100	mouse	Mammalia
<i>Rattus norvegicus</i>	RKR <u>K</u> RS	83	rat	
<i>Mesocricetus auratus</i>	RKR <u>K</u> RS	55	golden hamster	
<i>Ailuropoda melanoleuca</i>	RKR <u>K</u> RS	47	giant panda	
<i>Equus caballus</i>	RKR <u>K</u> RS	46	horse	
<i>Camelus bactrianus</i>	RKR <u>K</u> RS	46	camel	
<i>Vulpes vulpes</i>	RKR <u>K</u> RS	45	red fox	
<i>Canis lupus familiaris</i>	RKR <u>K</u> RS	45	dog	
<i>Lama glama</i>	RKR <u>K</u> RR	45	lama	
<i>Physeter catodon</i>	RKR <u>R</u> RS	44	sperm whale	
<i>Marmota monax</i>	RKR <u>K</u> RS	44	woodchuck	
<i>Bos taurus</i>	RKR <u>K</u> RS	44	cow	
<i>Felis catus</i>	RKR <u>K</u> RS	44	cat	
<i>Dasyopus novemcinctus</i>	RKR <u>K</u> RS	44	armadillo	
<i>Sus scrofa</i>	RKR <u>K</u> RS	44	pig	
<i>Moschus berezovskii</i>	RKR <u>K</u> RS	44	musk deer	
<i>Capra hircus</i>	RKR <u>K</u> RS	44	goat	
<i>Ovis aries</i>	RKR <u>K</u> RS	44	sheep	
<i>Bubalus carabanensis</i>	RKR <u>K</u> RS	44	water buffalo	
<i>Macaca mulatta</i>	GKR <u>K</u> RS	42	rhesus macaque	
<i>Macaca fascicularis</i>	GKR <u>K</u> RS	42	crab-eating macaque	
<i>Papio anubis</i>	GKR <u>K</u> RS	42	olive baboon	
<i>Tursiops truncatus</i>	RKR <u>R</u> RS	42	dolphin	
<i>Loxodonta africana</i>	SKR <u>K</u> RR	42	african elephant	
<i>Oryctolagus cuniculus</i>	KKR <u>K</u> RS	42	rabbit	
<i>Pongo abelii</i>	GKR <u>K</u> RS	41	sumatran orangutan	
<i>Gorilla gorilla gorilla</i>	GKR <u>K</u> RS	41	gorilla	
<i>Homo sapiens</i>	GKR <u>K</u> RS	41	human	
<i>Pan troglodytes</i>	GKR <u>K</u> RS	41	chimpanzee	
<i>Cavia porcellus</i>	RKR <u>R</u> RT	41	guinea pig	
<i>Heterocephalus glaber</i>	RKR <u>R</u> RS	38	naked mole rat	
<i>Phascolarctos cinereus</i>	RKR <u>K</u> RR	35	koala	
<i>Ornithorhynchus anatinus</i>	RKR <u>R</u> RS	29	platypus	
<i>Taeniopygia guttata</i>	YKR <u>K</u> RS	33	zebra finch	Aves
<i>Coturnix japonica</i>	SKR <u>K</u> RS	32	japanese quail	
<i>Phasianus colchicus colchicus</i>	SKR <u>K</u> RS	31	pheasant	
<i>Meleagris gallopavo</i>	SKR <u>K</u> RS	30	wild turkey	
<i>Gallus gallus</i>	FKR <u>K</u> RS	30	chicken	
<i>Columba livia</i>	LKR <u>K</u> RS	29	rock dove	
<i>Anas platyrhynchos</i>	SKR <u>K</u> RS	29	mallard	
<i>Pelodiscus sinensis</i>	NKR <u>K</u> RS	30	chinese soft-shelled turtle	Reptilia
<i>Alligator sinensis</i>	ER <u>R</u> RRQ	29	china alligator	Amphibia
<i>Rhinatrema bivittatum</i>	IR <u>K</u> KRS	29	two-lined caecilian	
<i>Xenopus tropicalis</i>	VKR <u>K</u> KL	25	tropical clawed frog	Amphibia
<i>Lithobates catesbeiana</i>	VRR <u>K</u> RG	22	american bullfrog	
<i>Oncorhynchus mykiss</i>	NRR <u>K</u> RR	27	rainbow trout	bony fish
<i>Salmon Salar</i>	NRR <u>K</u> RR	23	atlantic salmon	
<i>Labeo rohita</i>	ER <u>R</u> RRQ	22	carp	
<i>Danio rerio</i>	ER <u>K</u> RRQ	22	zebra fish	
<i>Callorhynchus milii</i>	GR <u>R</u> RRR	23	elephant shark	cartilaginous fish

Based on the FASTA Identifier of IFN $\gamma$  protein sequences from 50 different species, the overall sequence homology was determined using protein BLAST (NIH). The table was arranged based on sequence identity to mouse within a common taxon. Deviations from mouse KRKR motif are underlined. Common amino acid single-letter code is shown, e.g. R: Arginin, K: Lysin.

Based on the FASTA Identifier of IFN $\gamma$  protein sequences from 50 different species, the overall sequence homology was determined using protein BLAST (NIH). The table was arranged based on sequence identity to mouse within a common taxon. Deviations from mouse KRKR motif are underlined. Common amino acid single-letter code is shown, for example R: Arginin, K: Lysin.

## Reporting Summary

Nature Portfolio wishes to improve the reproducibility of the work that we publish. This form provides structure for consistency and transparency in reporting. For further information on Nature Portfolio policies, see our [Editorial Policies](#) and the [Editorial Policy Checklist](#).

### Statistics

For all statistical analyses, confirm that the following items are present in the figure legend, table legend, main text, or Methods section.

n/a Confirmed

- The exact sample size ( $n$ ) for each experimental group/condition, given as a discrete number and unit of measurement
- A statement on whether measurements were taken from distinct samples or whether the same sample was measured repeatedly
- The statistical test(s) used AND whether they are one- or two-sided  
*Only common tests should be described solely by name; describe more complex techniques in the Methods section.*
- A description of all covariates tested
- A description of any assumptions or corrections, such as tests of normality and adjustment for multiple comparisons
- A full description of the statistical parameters including central tendency (e.g. means) or other basic estimates (e.g. regression coefficient) AND variation (e.g. standard deviation) or associated estimates of uncertainty (e.g. confidence intervals)
- For null hypothesis testing, the test statistic (e.g.  $F$ ,  $t$ ,  $r$ ) with confidence intervals, effect sizes, degrees of freedom and  $P$  value noted  
*Give  $P$  values as exact values whenever suitable.*
- For Bayesian analysis, information on the choice of priors and Markov chain Monte Carlo settings
- For hierarchical and complex designs, identification of the appropriate level for tests and full reporting of outcomes
- Estimates of effect sizes (e.g. Cohen's  $d$ , Pearson's  $r$ ), indicating how they were calculated

*Our web collection on [statistics for biologists](#) contains articles on many of the points above.*

### Software and code

Policy information about [availability of computer code](#)

Data collection

Data analysis

For manuscripts utilizing custom algorithms or software that are central to the research but not yet described in published literature, software must be made available to editors and reviewers. We strongly encourage code deposition in a community repository (e.g. GitHub). See the Nature Portfolio [guidelines for submitting code & software](#) for further information.

### Data

Policy information about [availability of data](#)

All manuscripts must include a [data availability statement](#). This statement should provide the following information, where applicable:

- Accession codes, unique identifiers, or web links for publicly available datasets
- A description of any restrictions on data availability
- For clinical datasets or third party data, please ensure that the statement adheres to our [policy](#)

Fasta Identifiers of analysed IFN $\gamma$  sequences from different species can be found in supplementary information. Data from central experiments showing that IFN $\gamma$  binding to extracellular matrix prevents fatal systemic toxicity are provided as excel sheets in the supplementary information. We have provided a data availability statement.

## Field-specific reporting

Please select the one below that is the best fit for your research. If you are not sure, read the appropriate sections before making your selection.

Life sciences       Behavioural & social sciences       Ecological, evolutionary & environmental sciences

For a reference copy of the document with all sections, see [nature.com/documents/nr-reporting-summary-flat.pdf](https://www.nature.com/documents/nr-reporting-summary-flat.pdf)

## Life sciences study design

All studies must disclose on these points even when the disclosure is negative.

Sample size	Sample Size for animal experiment was determined based on the statistical calculations during the application for the respective license. Numbers of animals in the respective experimental group were then typically split into at least two independent experiments (biological replicates).
Data exclusions	No data was excluded.
Replication	Experiments were replicated at least twice if not stated otherwise.
Randomization	Mice were randomly assigned into groups when injected with tumor cells. For ATT experiments, mice were allocated to groups based on equal distribution in tumor size between different groups.
Blinding	Investigators were not blinded as endpoint criteria of mouse experiments were defined prior to experiments. Mice reaching endpoint criteria were analysed independently of their group allocation.

## Reporting for specific materials, systems and methods

We require information from authors about some types of materials, experimental systems and methods used in many studies. Here, indicate whether each material, system or method listed is relevant to your study. If you are not sure if a list item applies to your research, read the appropriate section before selecting a response.

### Materials & experimental systems

### Methods

n/a	Involved in the study	n/a	Involved in the study
<input type="checkbox"/>	<input checked="" type="checkbox"/> Antibodies	<input checked="" type="checkbox"/>	<input type="checkbox"/> ChIP-seq
<input type="checkbox"/>	<input checked="" type="checkbox"/> Eukaryotic cell lines	<input type="checkbox"/>	<input checked="" type="checkbox"/> Flow cytometry
<input checked="" type="checkbox"/>	<input type="checkbox"/> Palaeontology and archaeology	<input checked="" type="checkbox"/>	<input type="checkbox"/> MRI-based neuroimaging
<input type="checkbox"/>	<input checked="" type="checkbox"/> Animals and other organisms		
<input checked="" type="checkbox"/>	<input type="checkbox"/> Human research participants		
<input checked="" type="checkbox"/>	<input type="checkbox"/> Clinical data		
<input checked="" type="checkbox"/>	<input type="checkbox"/> Dual use research of concern		

## Antibodies

Antibodies used	<p>CD45.2 APC, 104, Biolegend 109814, Mouse IgG2a, k (1:100)            CD3 FITC, 145-2C11, BD Biosciences 553062, Armenian Hamster IgG1, k (1:20)            CD45.2 BV421, 104, Biolegend 109832, Mouse IgG2a, k (1:100)            CD19 FITC, 6D5, Biolegend 115506, Rat IgG2a, k (1:100)            CD11b BV510, M1/70, Biolegend 101263, Rat IgG2b, k (1:100)            CD11c FITC, HL3, BD Biosciences 553801, Hamster IgG1 (1:50)            NK1.1 APC, Miltenyi Biotec 130-102-350, (1:20)            RGS-His Antibody, 34650, Quiagen            H-2Kb/H-2Db-Biotin, 28-8-6, BD Biosciences 553575, (1:100)            Streptavidin-APC, BD Biosciences 554067, (1:200)            Heparan sulfate proteoglycan 2 antibody, A7L6, Abcam ab2501, (1:100)            goat anti-rat-Alexa568, Invitrogen A11077, (1:250)            CD146-Alexa647, ME-9F1, Biolegend 134702, (1:33)            Hoechst 33342, Sigma Aldrich            ultra-leaf-purified CD3, 145-2C11, Biolegend 100340, Armenian Hamster IgG1, k, (n.a.)            ultra-leaf purified Armenian Hamster IgG1, k isotype control, Biolegend 400940 (n.a.)            CD8 BV421, 53-6.7, Biolegend 100753, (1:50-1:100)            Vb7 PE, TR310, BD Biosciences 553216 (1:50)            CD3-APC, 145-2C11, Biolegend 100312 (1:50)            Surface staining LCMV Panel            CD4-APC/Fire750, RM4-4, Biolegend 116019, Rat IgG2b, k</p>
-----------------	---

CD8-BV510 53-6.7, Biolegend 100751, Rat IgG2a, k  
 KLRG-1-PerCP-Cy5.5, 2F1, BD 563595, Syrian hamster IgG  
 CD127-BV421, A7R34, Biolegend 135023, Rat IgG2a, k  
 CD44-APC, IM7, eBioscience 17-0441, Rat IgG2b, k  
 CD62L-BV650, MEL-14, Biolegend 104453, Rat IgG2a, k  
 PD-1-BV785, 29F.1A12, Biolegend 135225, Rat IgG2a, k  
 LAG3-PE-Cy7, C9B7W, Biolegend 125208, Rat IgG1, k  
 Tet-GP33-PE, Baylor College of Medicine  
 Tet-NP396-PE, Baylor College of Medicine  
 CD45.2-BV711, 104, Biolegend 109847, Mouse (SJL) IgG2a, κ 1:125  
 CD19-PE, 6D5, Biolegend 115508, Rat IgG2a, κ 1:250  
 CD4-PE-cy7, RM4-5, Biolegend 116016, Rat IgG2a, κ 1:250  
 CD8-FITC, 53-6.7, Biolegend 100706, Rat IgG2a, κ 1:250  
 CD3-BV421, 145-2C11, Biolegend 100336, Armenian Hamster IgG 1:125  
 CD274 (PD-L1)-APC, 10F.9G2, Biolegend 124312, Rat IgG2b, κ 1:250  
 Fc block, 93, Biolegend 101302, Rat IgG2a, λ  
 CD4 Fitc RM4-5, Biolegend 100510, Rat IgG2a, κ 1:250  
 CD8 BV421 53-6.7, Biolegend Rat IgG2a, κ 1:250  
 CD19 PE 6D5, Biolegend 100738, Rat IgG2a, κ 1:250  
 Mouse anti-Stat1 PE 4a, BD Biosciences 612564, Mouse IgG2a 1:5  
 Isotype control PE MOPC-173, BD Biosciences 558595, Mouse IgG2a, κ

Intracellular cytokine staining LCMV Panel  
 CD8-PerCP-Cy5.5, 53-6.7, Biolegend, Rat IgG2a, k  
 CD4-BV650, RM4-4, Biolegend, Rat IgG2b, k  
 IFN $\gamma$ -APC, XMG1.2, Biolegend, Rat IgG1, k  
 TNF-FITC, MP6-XT22, Biolegend, Rat IgG1, k

#### Validation

Antibodies were validated using the respective antigen on cells or expressed by cells and controlled by respective isotypes. For heparan sulfate staining, stainings without the primary antibodies served as controls. The Perlecan - heparan sulfate antibody was previously reported for mouse tissue staining: Tsiantoulas, D., et al. (2021). "APRIL limits atherosclerosis by binding to heparan sulfate proteoglycans." Nature 597(7874): 92+

## Eukaryotic cell lines

### Policy information about cell lines

#### Cell line source(s)

B16F10, MCA313, 16.113, HEK293T

#### Authentication

B16F10 cells were authenticated by IFN $\gamma$ -dependent upregulation of MHC I, as determined by flow cytometry, and pigmentation of the cells. MCA313 were identified based on their morphology (fibroblast-like) and by PCR specific for the neomycin resistance cassette within the inactivated IFN $\gamma$ R locus. In addition the expression of mouse MHC I was confirmed by flow cytometry. 16.113 cell line was identified based on IFN $\gamma$  secretion by TCR I - T cells (specific for the Large T antigen expressed by the tumor cells) upon co-culture. HEK293T were only used to produce retroviral vector particles and not in any experiments.

#### Mycoplasma contamination

All cell lines were routinely tested and were negative by PCR-Test for Mycoplasma.

#### Commonly misidentified lines (See ICLAC register)

*Name any commonly misidentified cell lines used in the study and provide a rationale for their use.*

## Animals and other organisms

### Policy information about studies involving animals; ARRIVE guidelines recommended for reporting animal research

#### Laboratory animals

Rag1<sup>-/-</sup> (B6.129S7-Rag1tm1Mom/J, 002216), TCR-I transgenic mice (B6.Cg-Tg(TcraY1,TcrbY1)416Tev/J, 005236), C57BL/6N (005304), C57BL/6J (000664), B6.129S7-Iifng<tm1Ts>/J (002287) and B6.129S7-Iifng1(tm1Agt)/J (003288) mouse strains were obtained from The Jackson Laboratory. For colocalisation experiments, male and female mice were used at 11-43 weeks of age. For local release of IFN $\gamma$ , male and female mice were used at 7-33 weeks of age. Female Rag1<sup>-/-</sup> mice were injected with cancer cells at 7-16 weeks of age. IFN $\gamma$ -delKRRR mice for LCMV Experiments were infected at 11-19 weeks. C57BL/6 mice from Janvier were aged and sex matched.  
 Arrive criteria were adhered to. 1. For each experiment the study design and controls are described. 2. Sample size was calculated beforehand with the application and if not indicated otherwise at least two biological replicates were performed to test reproducibility. 3. No animals were excluded. 4. Mice were randomly assigned into groups when injected with tumor cells. For ATT experiments, mice were allocated to groups based on equal distribution in tumor size between different groups. 5. No blinding was performed. 6. All outcome measures (for statistical analysis) are defined. The hypothesis are stated. 7. Statistical methods are described in the Text and M+M section. 8. Appropriate information on mice (genotype, sex, age, provenience, health – and immune status) is given. 9. Experiments and 10. Results are described.

#### Wild animals

*Provide details on animals observed in or captured in the field; report species, sex and age where possible. Describe how animals were caught and transported and what happened to captive animals after the study (if killed, explain why and describe method; if released, say where and when) OR state that the study did not involve wild animals.*

Field-collected samples

For laboratory work with field-collected samples, describe all relevant parameters such as housing, maintenance, temperature, photoperiod and end-of-experiment protocol OR state that the study did not involve samples collected from the field.

Ethics oversight

Landesamt für Gesundheit und Soziales, Berlin (G-322/10, G-114/17, G-0058/16)  
Regierungspräsidium Freiburg (G-15/168)

Note that full information on the approval of the study protocol must also be provided in the manuscript.

## Flow Cytometry

### Plots

Confirm that:

- The axis labels state the marker and fluorochrome used (e.g. CD4-FITC).
- The axis scales are clearly visible. Include numbers along axes only for bottom left plot of group (a 'group' is an analysis of identical markers).
- All plots are contour plots with outliers or pseudocolor plots.
- A numerical value for number of cells or percentage (with statistics) is provided.

### Methodology

Sample preparation

Blood: whole blood was collected in K2-EDTA Tubes and subjected to Fc Block for 5-10 minutes, followed by 20 min incubation with antibody mixtures in PBS. ACK lysis was performed, samples were washed twice before acquisition. Cancer cells from cell culture: Cells were detached using trypsin or a cell scraper and washed with PBS. Splenocytes: Spleens were excised and single cells suspension were generated using a 40µm cell strainer. Suspensions were subjected to ACK Lysis. Stainings were performed similar to blood stainings.

Instrument

MACSQuant Analyzer, Milteny  
Facs Calibur, BD Biosciences  
Aria Fusion Cell Sorter, BD Biosciences  
LSR Fortessa cytometer (BD Biosciences)

Software

FlowJo 8.8.7 & 10, BD Diva,

Cell population abundance

MCA313 cells were single cell sorted.

Gating strategy

Data involving cell lines were gated on FSC/SSC, followed by gating for the analysed markers. Boundaries between positive and negative populations were set based on FMO controls or cell lines negative for the specific markers. Dead cells were excluded from analysis.  
For characterization of splenocytes from IFNg-delKRKR mice, FCS/SSC was followed by CD45.2-positive selection and subsequent analysis of respective surface markers. Isotype controls were used to set boundaries.  
Blood lymphocytes were gated based on FSC/SSC, followed by discrimination between CD3 negative and positive, based on isotype control. The CD3-positive fraction was then analysed for CD8 and Vb7 staining. For Vb7 boundaries, the isotype was used. In all cases, isotype controls were performed on the same samples as the primary staining.

- Tick this box to confirm that a figure exemplifying the gating strategy is provided in the Supplementary Information.